Gondwana Research, V. 7, No. 3, pp. 771-790.

ISSN: 1342-937X

GR Gondwana Research

Fragments of Vendian-Early Carboniferous Oceanic Crust of the Paleo-Asian Ocean in Foldbelts of the Altai-Sayan Region of Central Asia: Geochemistry, Biostratigraphy and Structural Setting

I.Yu. Safonova[1], M.M. Buslov[1], K. Iwata[2] and D.A. Kokh[1]

[1] *United Institute of Geology, Geophysics and Mineralogy, Russian Academy of Sciences, Siberian Branch, 630090, Koptyuga ave. 3, Novosibirsk, Russia, E-mail: inna@uiggm.nsc.ru*

[2] *Division of Earth and Planetary Sciences, Graduate School of Science, Hokkaido University, 060-0810, Sapporo, Japan*

(Manuscript received March 25, 2003; accepted November 11, 2003)

Abstract

Detailed geological, geochemical and biostratigraphic studies of rocks from basaltic-sedimentary terranes in the Kurai and Katun accretionary wedges (Vendian-Middle Cambrian units), the Charysh-Terekta strike-slip zone (Late Cambrian-Early Ordovician units), and the Chara ophiolite-bearing strike-slip zone (Late Devonian-Early Carboniferous units) have been undertaken. The Early Cambrian accretionary wedges record a stage of the Kuznetsk-Altai island arc evolution. The Charysh-Terekta strike-slip zone records evidence of the Late Devonian collision of the Gondwana-derived Altai-Mongolian terrane and the Siberian continent. The Chara ophiolitic zone was formed during the Late Carboniferous-Permian collision of the Siberian and Kazakhstan continents.

Our study of these fragments of oceanic crust led us to conclude that intra-plate volcanism was active at the early stages of the Paleo-Asian oceanic evolution, in a period from the Vendian to the Early Carboniferous. Fragments of weakly to strongly differentiated oceanic and island-arc basalts have been preserved in accretion-collision zones and give information about chemical composition, petrology and tectonic setting of the oceanic crust at these times. The geochemical data indicate that the Altai and East Kazakhstan metabasalts could have been formed at mid-oceanic ridges, oceanic islands or oceanic plateau of the Paleo-Asian Ocean. Our interpretation of structural, lithological, geochemical and biostratigraphic data shows that the structure and composition of the oceanic lithosphere of the Paleo-Asian Ocean were similar to those of the present Pacific Ocean.

Key words: Vendian-Early Phanerozoic, Paleo-Asian Ocean basalts, geochemistry, biostratigraphy, Central Asia.

Introduction

The universally accepted idea that fragments of paleo-oceanic lithosphere are preserved in foldbelts was proved in previous studies, which showed that various types of ophiolites had been identified as oceanic crust fragments (Coleman, 1977; Dobretsov and Zonenshain, 1985). In recent years, numerous oceanic crust fragments have been found and identified in foldbelts of different ages.

In present-day oceanic basins, oceanic islands and basaltic plateaux occupy a significantly larger territory and volume than oceanic island arcs (Dobretsov et al., 2003). Therefore, fragments of these structures should be at least as widely present in fold belts as are island arc fragments. That they are less common in fold belts may be explained by the fact that they are subducted, or by difficulties in their recognition in structures comprising numerous tectonically mixed sedimentary and basaltic-sedimentary terranes. The preservation potential of fragments of oceanic islands and oceanic plateaus has been discussed in many publications (e.g., Ben-Avrahem et al., 1981; Chekhovich 1997; Dobretsov et al., 2003).

Three areas of the Altai-Sayan foldbelt will be considered: the Gorny Altai accretionary wedges of Early Cambrian age (Kurai and Katun), the Charysh-Terekta strike-slip zone of Late Devonian age (north-western Altai) and the Chara ophiolitic strike-slip zone of Late Devonian-Early Carboniferous age (East Kazakhstan) (Fig. 1). The Kurai and Katun accretionary wedges, which are probably fragments of oceanic islands, have been described in many publications (e.g., Buslov et al., 1993; Watanabe et al., 1993; Buslov and Watanabe, 1996; Dobretsov et al., 2003). The oceanic crust in the Charysh-Terekta and Charastrike-slip zones (the Zasurin Unit and the Chara ophiolitic belt, respectively) was discussed by Buslov et al. (1999, 2000,

2001). Biostratigraphy of associated oceanic siliceous sedimentary rocks was reported in Iwata et al. (1994, 1997a, 1997b). This paper reviews the data on the previously recognized oceanic crust of Vendian-Early Carboniferous age formed in different structural settings, and presents new information on its chemical composition.

Geological Background

The tectonic structure of the Altai-Sayan foldbelt is a collage of terranes of different ages separated by numerous large-scale thrusts, strike-slip faults and nappes (Dobretsov and Zonenshain, 1985; Zonenshain et al., 1990; Buslov et al., 1993, 2003; Berzin and Dobretsov, 1994; Dobretsov et al., 1995;). The terranes are classified mainly based on Vendian-Cambrian geodynamic units of the Paleo-Asian Ocean. Figure 1 shows the major structural units that form a part of the Central Asian foldbelt, within the area between the Kazakhstan and Siberian continental blocks. The tectonic pattern of the Altai-Sayan area includes three groups of structural and tectonic units: (1) the Gondwana-derived Altai-Mongolian terrane; (2) terranes of different ages – Kalba-Narym, Rudny Altai, Gorny Altai – composed of fragments of Caledonian and Hercynian accretion-collision zones. Accretionary prisms (wedges) consist of fragments of subducted terranes of oceanic lithosphere – ophiolites, seamounts and ocean islands – which were accreted to island arcs and/or active continental margins; (3) systems of strike-slip faults and thrusts of different ages – Chara, Irtysh, North-East, Charysh-Terekta, Kurai, Teletsk-Bashkauss – separating collisional terranes from the margins of collided continents. Strike-slip deformation commonly completes the formation of suture zones, and/or they develop as intra-continental shear zones parallel to the ophiolitic sutures. The reactivated suture zones along the terrane fault boundaries – both sinistral and dextral – are composed not only of Vendian-Cambrian geodynamic units, but also of igneous, metamorphic and sedimentary rocks of Devonian and Carboniferous age (Buslov et al., 2001). These reactivated suture zones extend continuously along major faults beyond the terrane boundaries. The Chara fold zone, the Rudny Altai terrane and surrounding areas represent a Carboniferous-Permian junction structure between the Kazakhstan and Siberian continents. The northwestern part (Charysh and Inya areas) of the Gorny Altai terrane belongs to a reactivated suture zone which extends into the Gondwana-derived Altai-Mongolian terrane (Fig. 1).

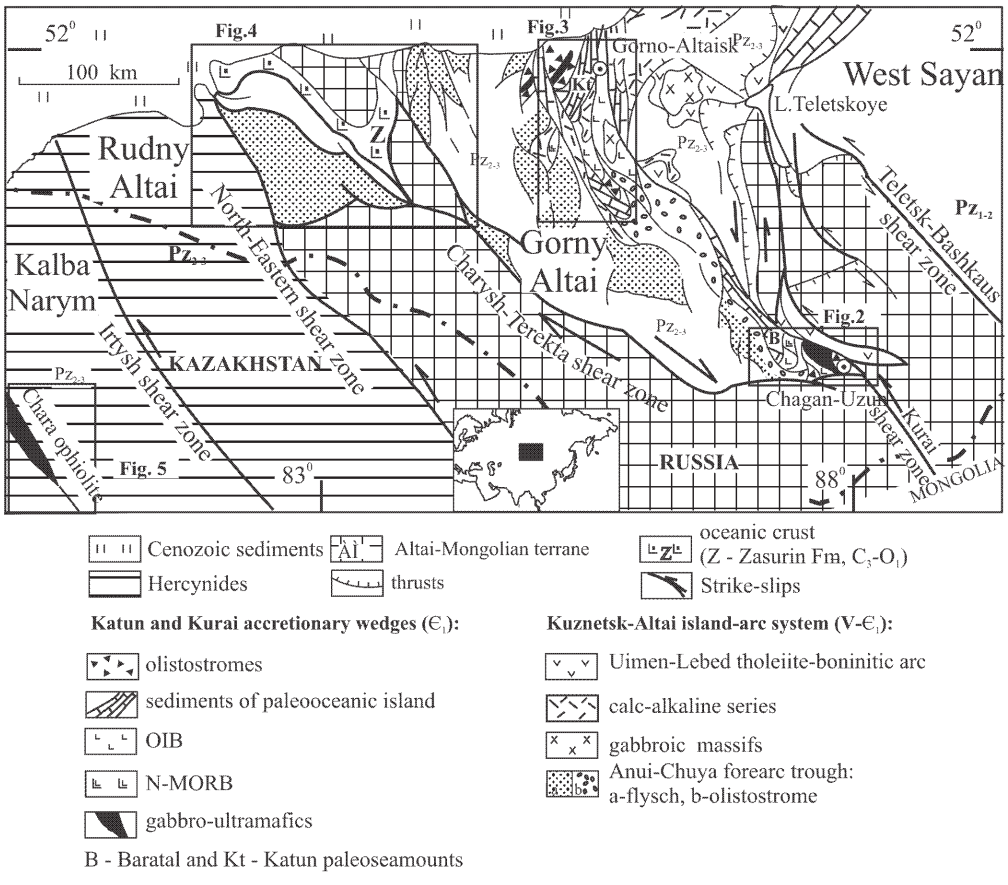

Fig. 1. Location and regional geology of Gorny Altai and North-West Altai.

Analytical Methods and Geochemical Approaches

Metabasalts for geochemical study were collected from all localities considered in this paper. Samples were taken from least deformed and altered outcrops with few or no veinlets or vesicles. In all samples analyzed, olivine, pyroxene and volcanic glass had been replaced by chlorite and epidote, and most plagioclase was albitized. All analyses were made at the United Institute of Geology, Geophysics and Mineralogy, SB RAS. Major elements and some trace elements (Rb, Sr, Y, Zr, Nb) were determined using a "Nauchpribor" X-Ray Fluorescence Spectrometer (analytical procedure following Russian state analytical standard OST-41-08-212-82 Mingeo SSSR). REE and other trace elements were analyzed with the neutron-activation gamma-rays method (INAA) by V.A. Bobrov using Ge detectors for γ-rays higher that 30 KeV and below 2000 KeV (REE and HFSE), Atomic Absorption Spectrometry (LILE) using a 3030 AA spectrometer, and XRF (Rb, Sr, Y, Zr, Nb).

Most interpretations are based on REE and trace elements, because most major elements are highly mobile during post-magmatic sea-floor alteration and metamorphism. Na, Ka and low-field-strength elements are mostly mobile during alteration (e.g., Humphris and Thompson, 1978), whereas HFSE and REE are essentially immobile even during the most severe sea-floor hydrothermal metamorphism (e.g., Wood et al., 1979). Therefore, only immobile HFSE and REE were used to identify the magmatic affinity and petrogenesis of these altered mafic volcanic rocks. The abundances of rare-earth elements (REE) have been used to evaluate the petrogenesis of basalts. Thus, we utilized diagrams which are based upon immobile trace elements. The diagrams below use high field strength elements (HFSE) such as Ti, Zr, Y, Nb and several others that are also thought to be relatively immobile in aqueous fluids unless there are high activities of F^- (not observed in our case). This means that these elements will be stable under conditions of hydrothermal alteration, sea-floor weathering, and up to medium-grade metamorphism (mid-amphibolite facies) (Rollinson, 1993).

The Nb/Y ratio was used for the distinction of alkaline and subalkaline series (Winchester and Floyd, 1977). MORB-normalized trace element patterns (McDonough and Sun, 1995) and 2Nb-Zr/4-Y systematics (Meschede, 1986) were utilized to identify tectonic setting of formation. Nb/Y-Nb/Zr diagram was used to compare with superplume-related oceanic island basalts (Tatsumi et al., 1998).

Gorny Altai Accretionary Wedges: Vendian-Early Cambrian Oceanic Crust

The Gorny Altai terrane contains a complete set of Vendian-Cambrian rocks (Buslov et al., 2002). Previous petrochemical studies by Buslov et al. (1993, 1998, 2001) deciphered the tectonic settings of volcanic rocks. A number of Early Cambrian accretionary units including OIB and N-MORB and Vendian-Cambrian island arc units have been recognized, and these contact each other in the Kurai (west of Chagan-Uzun Village) and Katun (nearby Gorno-Altaisk city) zones of the Gorny Altai (Buslov et al., 1998; Watanabe et al., 1993; Simonov et al., 1994; Buslov and Watanabe, 1996; Buslov et al., 2001).

Study of the geodynamic units which are best observed in the Kurai (South-Eastern Altai) and Katun (Central Altai) zones made it possible to reconstruct the paleo geodynamic processes (subduction and accretion), which seem to be similar to those in the western part of the Pacific active margin (Watanabe et al., 1993; Buslov and Watanabe, 1996).

Kurai accretionary wedge

Structural position

The Kurai accretionary wedge is located in the southeastern Gorny Altai (Fig. 2). It has been thoroughly studied in recent years (e.g., Buslov et al., 1993, 1998, 2001, 2002; Buslov and Watanabe, 1996; Dobretsov et al., 2003). Fragments of the accretion-collision complexes have been almost completely preserved there. The Baratal oceanic island collided with an island arc and locked the subduction zone, resulting in exhumation of the eclogites, blueschists, garnet amphibolites and metaperidotites of the Chagan-Uzun massif (Buslov et al., 1993; Buslov and Watanabe, 1996). The accretionary wedge hosts slivers of the Baratal oceanic island of variable composition and size. The slivers comprise oceanic sediments and oceanic island basaltic units, Chagan-Uzun oceanic ophiolites and serpentinitic mélange, along with slivers and minor blocks of eclogite, garnet amphibolite and actinolite schists. The occurrence of these metamorphic rocks is a characteristic feature of the Kurai accretionary prism. In the Middle-Late Paleozoic, the accretionary prism was folded.

The Baratal oceanic island comprised three types of rocks: (1) basaltic rocks, (2) alternation of volcanic and sedimentary rocks, and (3) reef limestone. The basaltic rocks are mainly dark-gray and gray-green pillow-lavas and variolitic lavas, with subordinate amounts of amygdaloidal sub-alkaline andesitic basalts, diabase and gabbro-diabase dikes and sills. The magmatic rocks are associated with sparse lenses of dark-gray and gray limestone, dolomite, black and gray cherts and rarely volcaniclastic sandstone.

The Kurai accretionary wedge comprises metamorphic rocks and ophiolitic assemblages, as typified by the section

exposed south of Kurai (Fig. 2). Boudinaged and deformed gabbro, gabbro-diabase, and diabase dykes cut the lower ophiolitic thrust sheet. These are compositionally similar to the Early-Middle Cambrian calc-alkaline island-arc series, and represent the upper age limit of exhumation (Buslov et al., 2002).

In general, according to its structural position, rock assemblages, and major and trace element chemistry, the Baratal terrane can be regarded as an oceanic island with a fragment of the oceanic crust at its base.

Biostratigraphy

In the Kurai area, massive limestone and limestone breccias conformably overlap metabasalts. The limestone and associated metabasalts are called the Baratal paleo-seamount. The limestones include stromatolites, microphytolites and ooids that suggest a Vendian age and a shallow-marine environment. All types of the limestone lack coarse-grained terrigenous clastic material. The limestone breccia contains clasts of micritic limestone, metabasalts and chert. Poor grading, poor sorting and thin bedding suggest that the limestone breccia formed as sediment-gravity-flow (debris flow) deposits. In addition, laminated limestones and bedded micritic limestones are associated with the limestone breccia. The associated metabasalts have geochemistry similar to those of modern oceanic island basalts (see below) and we therefore suggest that the overlying limestone was formed on and around an ancient seamount or paleo-plateau (Uchio et al., 2001; Dobretsov et al., 2003).

The limestones in the area under consideration are lithologically classified into four types: (1) massive limestone, (2) laminated limestone, (3) micritic limestone, and (4) limestone breccia. The absence of terrigenous clastic detritus indicates that all the limestone types were deposited in a mid-oceanic environment.

The depositional sites of these four types of limestone lithologies are inferred as follows. The Type 1 massive and micritic limestones with shallow-water stromatolite are inferred to have formed on the top of a paleo-seamount (paleo-plateau). Type 2 laminated limestone corresponds to allodapic limestone (limestone turbidite) accumulated at the base of paleo-seamount slopes, and Type 3 micritic limestone is thought to have been deposited at the bottom of the paleo-seamount. Type 4 limestone breccia represents debris flow deposits accumulated on the slopes or at the base of the slopes of the paleo-seamount (Uchio et al., 2001).

Geochemistry of basaltic rocks

Selected chemical analyses of Kurai metabasaltic rocks are presented in table 1. These are bulk rock chemical compositions of 11 metabasalts from the Kurai accretionary wedge. The metabasalts in this unit are dominated by fine- to medium-grained amygdaloidal basalt and andesitic basalt with porphyritic texture. The

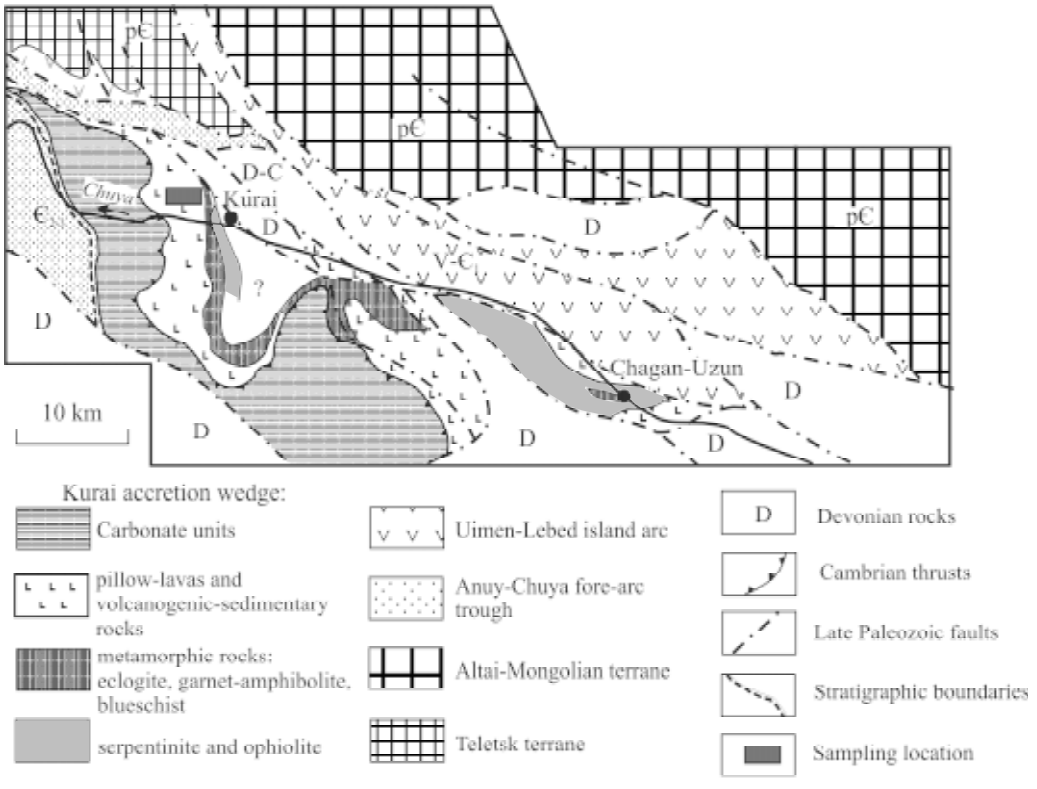

Fig. 2. Geological map of the Kurai accretionary wedge and surrounding geological units.

amygdales are filled by calcite and chlorite, and the phenocrysts are plagioclase and clinopyroxene. Groundmass is variolitic or hyalopilitic. These chemically uniform samples have been metamorphosed to the greenschist facies. All are subalkaline basalts, as shown by their low Nb/Y ratios (Fig. 6). FeO* wt.% tends to increase with increasing FeO*/MgO, suggesting a tholeiitic trend (Fig. 7A). The increase of TiO_2 with increasing FeO*/MgO is not so obvious, suggesting a character intermediate between abyssal tholeiite and island-arc tholeiite (IAT) (Fig. 7B). TiO_2 and P_2O_5 contents range from 0.43 wt.% to 2.3 wt.% and from 0.1 wt.% to 0.58 wt.%, respectively (Table 1). These characteristics are close to those of greenstones from the Idonnappu accretionary zone in the Urakawa area, southern central Hokkaido (Ueda et al., 2000). Al_2O_3 ranges from 13 wt.% to 18 wt.%. Average abundance is a little lower than in IAT, but is similar to greenstones from the Idonnappu zone. In general, compared to IAT Kurai metabasalts are depleted in LILE (K, Rb, Ba) and have similar or slightly greater HFSE (Zr, Nb, Th, Hf) contents. MgO and Cr_2O_3 are strongly influenced by crystal fractionation and are higher in IAT, confirming the difference between IAT and oceanic tholeiites.

Three groups of samples may be recognized according to their HFSE and LILE concentrations and Zr/Nb ratios. The first group possesses chemical characteristics of N-MORB. This includes samples 141, 146, 155, 170, which are enriched in HFSE and have Zr/Nb ratios much greater than 20 (Table 1; Wilson, 1989). The second group has OIB affinity, and includes a Th-rich and Hf- and Y-depleted sample (169) with a low Zr/Nb ratio (<20). The third group includes chemically intermediate samples 147, 154,

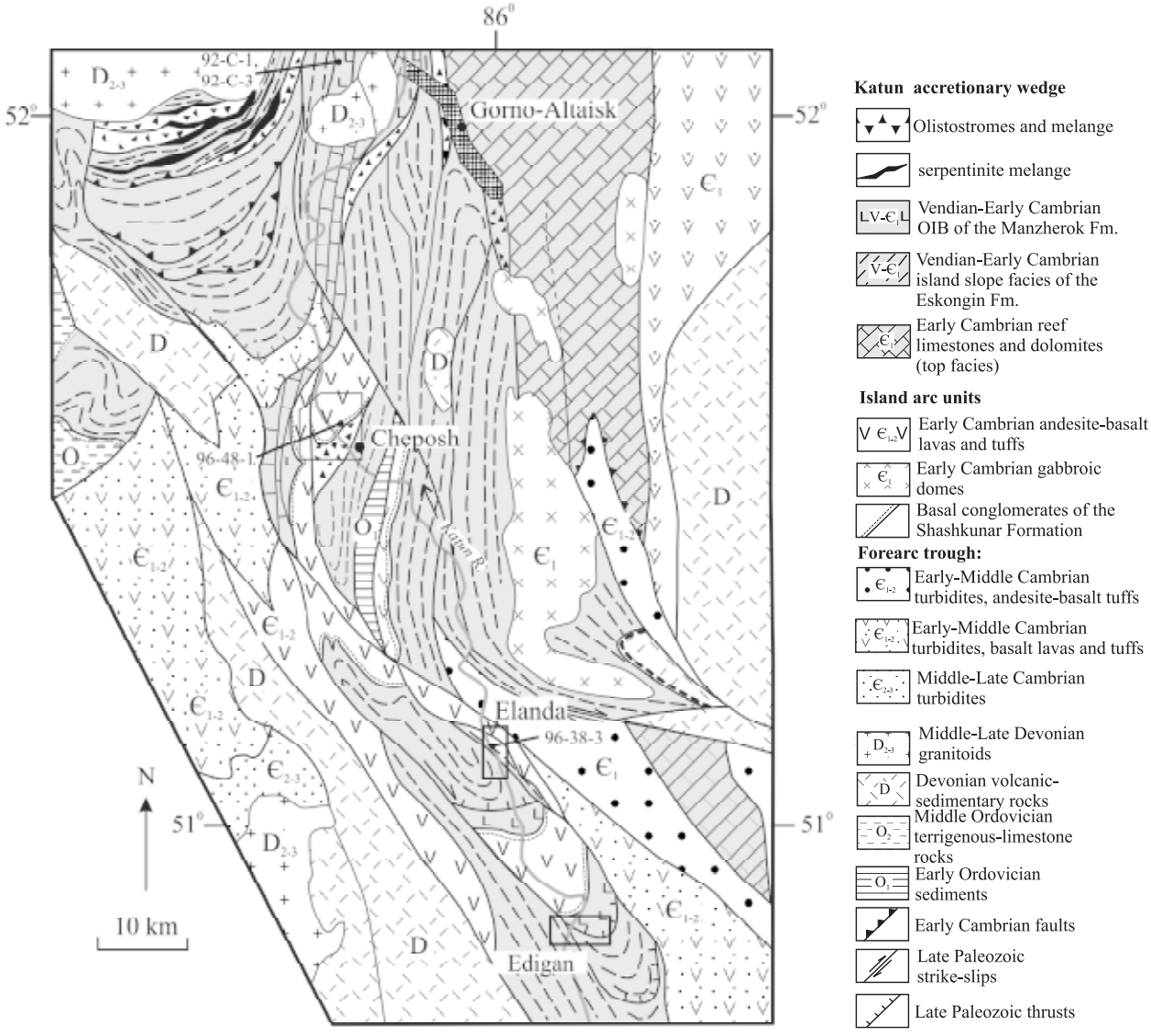

Fig. 3. Geological map of the Katun accretionary wedge.

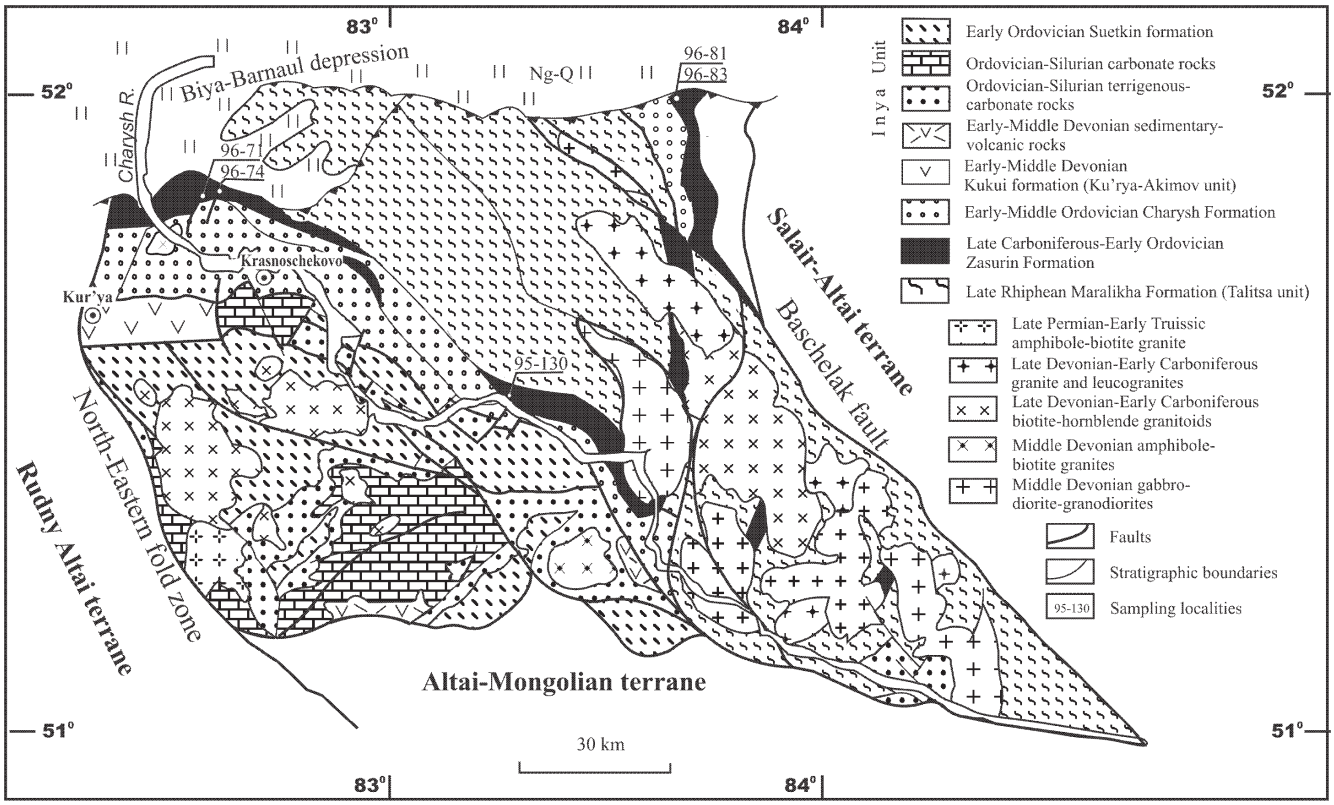

Fig. 4. Geological map of the Charysh-Terekta strike-slip zone in the north-western Gorny Altai (modified from Buslov et al., 2001).

158, 161, 165 and 96-56-1, which we interpret as T-MORB or oceanic plateau basalts (OPB) (Table 1, Frolova and Burikova, 1997; Ueda et al., 2000; Wilson, 1989). In the Nb-Zr/4-Y diagram (Fig. 8) sample 169 plots between the N-MORB and plume-type MORB (P-MORB) fields, like transitional-type MORB. All other samples plot in the field of N-MORB.

All but two (nos. 169 and 96-56-1) basaltic samples

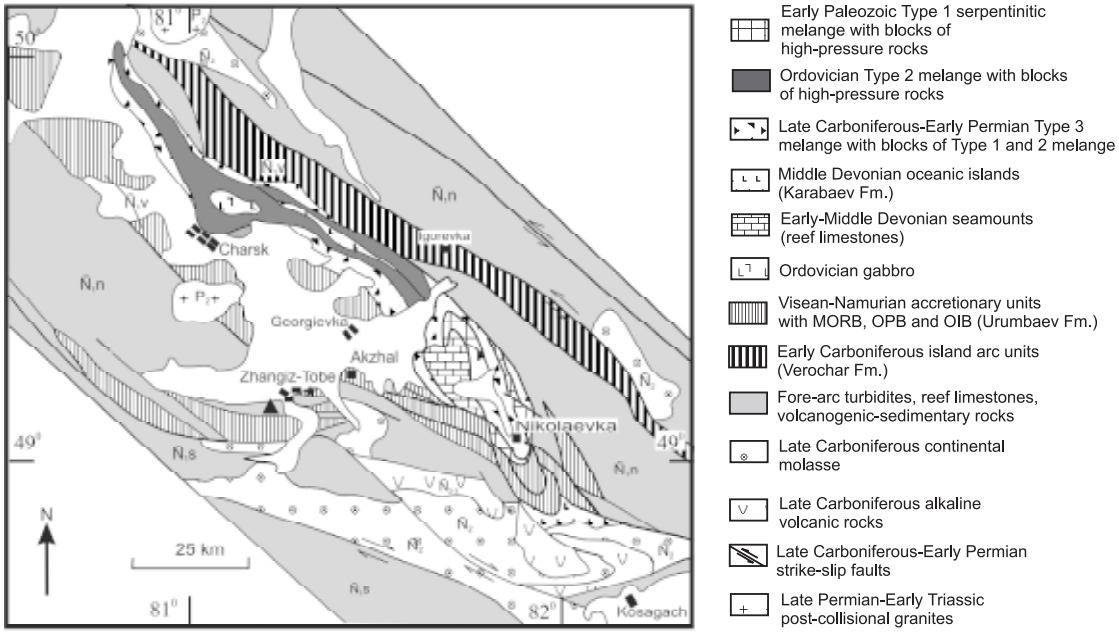

Fig. 5. Geological map of the Chara zone (modified from Buslov et al., 2001).

Table 1. Major and trace element analyses of volcanic rocks from the Kurai accretionary wedge.

Sample	141	146	147	154	155	158	161	165	169	170	96-56-1	N-MORB	OIB
SiO_2	49.59	47.25	49.18	46.27	52.36	47.61	47.53	47.29	48.89	48.51	50.15	49.13	46.46
TiO_2	1.23	1.84	1.75	2.36	1.84	1.54	1.78	1.65	0.43	1.45	1.511	1.17	3.01
AL_2O_3	14.14	13.67	13.10	12.90	14.17	14.67	16.15	14.60	17.86	13.44	14.57	15.64	14.64
Fe_2O_3	14.34	12.91	12.85	14.96	11.24	12.30	12.33	13.57	8.82	14.38	13.76	9.97	9.85
MnO	0.44	0.23	0.24	0.25	0.17	0.27	0.21	0.21	0.18	0.24	0.26	0.16	0.14
MgO	6.01	7.26	6.94	6.96	4.59	6.59	7.25	6.69	6.23	5.92	3.89	8.22	8.19
CaO	4.91	10.00	8.67	6.82	6.32	4.80	5.24	6.95	8.06	6.37	5.44	11.84	10.33
Na_2O	2.92	3.32	4.23	5.18	4.76	5.32	4.44	4.28	4.75	6.21	5.76	2.40	2.92
K_2O	1.50	0.29	0.36	0.49	0.70	0.54	0.44	0.44	0.90	0.21	0.71	0.20	0.84
P_2O_5	0.13	0.18	0.18	0.23	0.21	0.45	0.43	0.37	0.40	0.10	0.58	0.12	0.37
L.O.I.	5.41	2.74	2.37	3.35	2.53	5.42	3.71	3.59	3.13	3.07	3.86	1.09	-
Total	100.63	99.68	99.87	99.78	98.89	99.51	99.51	99.63	99.65	99.90	100.54		
La	4.6	5.7	2.8	6.5	5.9	7.5	8	7.2	20	3.2	11	2.50	37
Ce	12	16.5	7.4	15.5	18.5	18.6	20.6	16.6	42	8.5	25	7.50	80
Nd	7.7	13.2	5.3	12.3	13.7	12.8	15.6	11.4	19.9	6.8	16	7.30	38.5
Sm	2.75	4.4	2.1	4.7	4.6	4.3	4.2	3.6	4.1	2.65	5.2	2.63	10
Eu	1.1	1.7	0.83	1.65	1.75	1.8	1.88	1.77	1.3	1	2	1.02	3
Tb	0.62	1.09	0.5	0.94	1.11	0.74	0.8	0.74	0.41	0.57	1.1	0.67	1.05
Yb	3.2	5	2.15	3.4	4.7	2.7	2.9	2.8	1.4	2.7	3.8	3.05	2.16
Lu	0.56	0.8	0.35	0.6	0.77	0.4	0.43	0.41	0.22	0.48	0.55	0.46	0.3
Sc	32	41	45	38.6	31.3	24	29.3	27	24	38	19	40	
Th	0.38	0.25	0.45	0.35	0.25	0.45	0.5	0.4	0.85	0.18	0.9	0.12	4
U	0.47	0.2	0.3	0.05	0.04	0.2	0.28	0.13	0.04	0.04		0.05	1.02
Hf	2.1	3.6	1.4	2.9	3.9	1.9	2.1	1.6	0.8	1.6	2	2.05	7.8
Ta	0.12	0.22	0.1	0.23	0.2	0.21	0.21	0.16	0.1	0.04	0.25	0.13	2.7
Ba	280	10	50	70	100	260	600	70	300	10	480	6.30	350
Co	39	53	47	52	38	38	39	40	24	51	32		
Cr	10	100	251	40	25	75	8.5	7.5	10	9.5		250	
Rb	34.2	3.11	5	5.46	6.84	6.27	6.45	5.8	17.5	2.79	15	0.56	31
Sr	289	211	255	148	171	327	475	514	852	201	560	90.00	660
Y	35.7	58	28	48.8	61	35.2	38.2	32.6	15.45	35.5	40	28.00	29
Zr	75	157	62	137	186	78	99	72	38.5	73	108	74.00	280
Nb	1.7	4	2.2	5	4.5	3.7	4.3	3	4	1	4	2.3	48
Zr/Nb	43.86	38.86	27.56	27.13	41.06	21.20	23.02	23.53	9.63	72.28	27.00	31.76	5.83
$(Nb/La)_N$	0.35	0.67	0.76	0.73	0.72	0.46	0.51	0.40	0.19	0.30	0.34	0.78	1.42
$(La/Ta)_N$	2.33	1.58	1.70	1.72	1.79	2.17	2.32	2.74	12.16	4.86	2.67	1.14	0.71
$(La/Yb)_N$	0.91	0.72	0.83	1.21	0.80	1.76	1.75	1.63	9.08	0.75	1.84	0.62	10.29

Major elements are in wt.% and trace elements in ppm. Major elements in N-MORB are those of the average tholeiitic MORB from Wedepohl, 1981; Major elements in OIB are those of the Hawaian average subalkaline Ol-basalt (Frolova and Burikova, 1997). Trace elements in N-type MORB and OIB are concentrations from Sun and McDonough, 1989.

have very uniform REE patterns (Fig. 9), showing no obvious LREE enrichments with La_N = 9–25, $(La/Yb)_N$ = 0.15–1.9. Samples 147 and 170 have the lowest LREE. Four samples (158, 161, 165, 169) show small positive Eu anomalies. Sample 169, the most differentiated basalt, has the highest LREE abundances but the lowest HREE relative to the basalts, with La_N = 60, $(La/Yb)_N$ = 9.1 and a small positive Eu-anomaly. Sample 96-56-1 has elevated LREE and intermediate HREE with La_N = 33, $(La/Yb)_N$ = 1.9 and a small positive Eu-anomaly. This sample is transitional between sample 169 and the other samples. The other samples show relatively flat REE patterns and lack Eu anomalies, resembling those of Nauru and Ontong Java OPB (Fig. 9).

MORB-normalized trace element patterns show that HFSE and Nb abundances are almost equal to N-MORB (Fig. 10). These patterns also resemble those of oceanic plateau basalts (OPB) in the Nauru basin (Saunders, 1986; Floyd, 1989). The basalts are enriched in LILE and LREE relative to MORB, showing the signature of oceanic island basalt (OIB) (Pearce, 1982). Most samples have similar patterns and represent so-called transitional MORB (T-MORB) (Wilson, 1989). Sample 169 has the lowest HFSE, possibly due to extraction of HFSE-bearing phases from the melt, i.e. during melting of a subducted oceanic plate consisting of Mg-rich tholeiite, or due to special conditions in the magma chamber favorable for crystallization of HFSE-rich minerals, e.g., presence of rutile or ilmenite in the residual mantle. Most samples are depleted in Cr. This may be explained by fractionation of Cr-spinel from the melt.

In the chondrite-normalized spidergrams (Fig. 11; Sun and McDonough, 1989) all basaltic samples have "humped" patterns, probably due to LILE added during

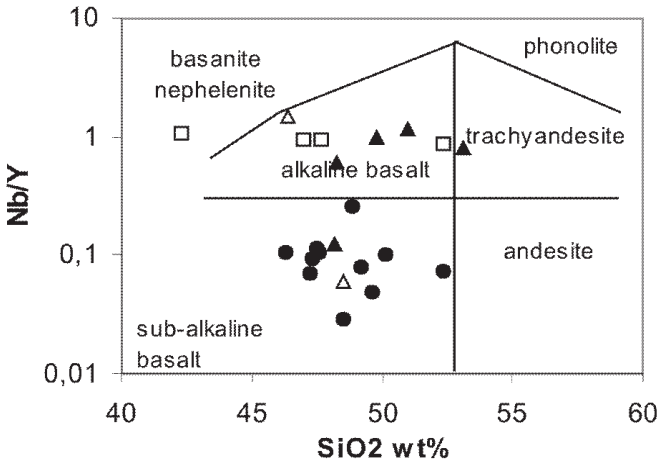

Fig. 6. Nb/Y vs SiO_2 classification diagram. Symbols - filled circles: Kurai metabasalts, open squares: Katun metabasalts, filled triangles: Zasurin metabasalts, open triangles: Chara metabasalts.

secondary alteration, and are characterized by variable enrichment in all the trace elements with respect to chondrite. These samples display mild depletion in Nb-Ta relative to La (i.e., $Nb/La_N < 1$, Table 1), unlike continental rift basalts or oceanic island lacking appreciable crustal contamination. Nevertheless, despite the Nb-Ta depletions, we cannot suggest crustal contamination was a factor in their petrogenesis because of their low Th abundances (Table 1, Fig. 11). The most differentiated basalts (169 and 96-56-1) also show mild Nb-Ta depletion ($(Nb/La)_N$ = 0.19 and 0.34, respectively) and very low Th (0.85 and 0.9 ppm, respectively). These special geochemical features are unlikely to have resulted from sialic crustal contamination, but rather from mafic lower crust or lithospheric mantle (Li et al., 2002), or they could also be from tapping a depleted mantle source. In addition, rather high alkali and LILE contents and moderate Nb depletion may suggest interaction between a mantle plume and a spinel-facies mantle source.

The Kurai samples plot in the MORB field on the Nb/Y versus Nb/Zr diagram, but sample 169 plots closer to the OIB field. In the Nb/Th versus Ti/Yb diagram, the samples form a trend extending from OIB to CLM (continental lithosphere mantle), suggesting mixing or contamination with lithospheric mantle (Fig. 12).

Thus, our data indicate that the Kurai metabasalts were possibly formed within oceanic islands, mid-oceanic ridges and/or oceanic plateaux. Low HFSE and flat patterns of most samples are best matches for T-MORB or OPB, which are quite different from OIB. Existence of a voluminous carbonate facies suggests a large oceanic edifice, thus supporting the proposal of an oceanic plateau rather that an oceanic spreading center. All the lavas show the low-temperature greenschist facies of regional metamorphism and sea-floor metamorphism (see also Gusev, 1991; Buslov et al., 1993, 2001).

Katun accretionary wedge

Structural position

The Katun accretionary wedge is situated north of the Kurai accretionary wedge and extends over a distance of more than 120 km along the Katun River, south of Gornoaltaisk (Fig. 3). It contains three types of paleo-oceanic island rock units: (1) limestones, black cherts, dolomites, siliceous shales, and thin basaltic flows; (2) high-Ti tholeiites and alkali basalts as described below; (3) reef limestone and dolomite. These units are thought to be fragments of a single unit formed in an oceanic island setting (Dobretsov et al., 2003). Volcanogenic, siliceous-limestone and carbonate paleo-oceanic units extend northeast to Gornaya Shoriya, and form a 40 x 250 km structure. In the northwestern part of the Katun accretionary wedge, the tectonic sheets and olistostromes

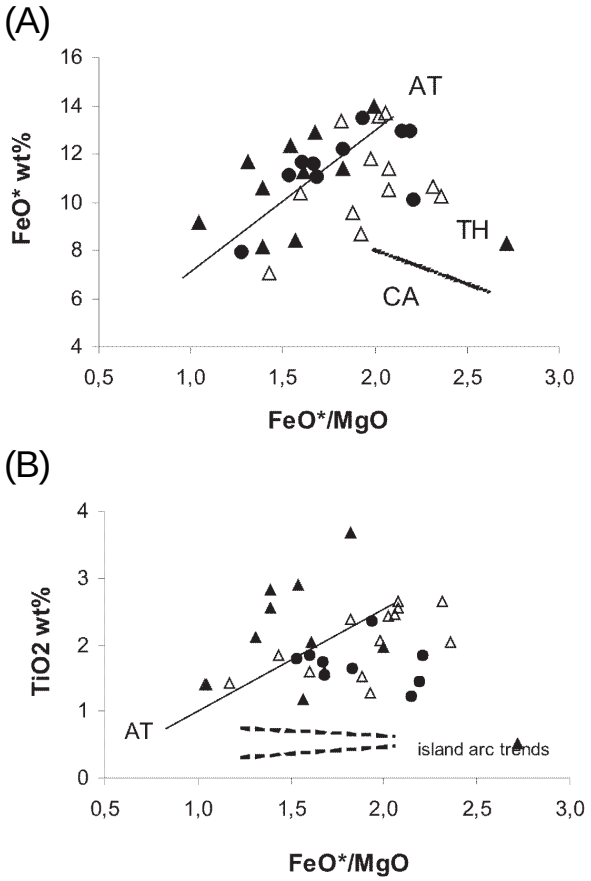

Fig. 7. Major element plots: (A) FeO* vs FeO*/MgO; (B) TiO_2* vs FeO*/MgO. Discriminant fields and trends of abyssal tholeiite (AT), tholeiite (TH) and calc-alkaline volcanic rocks (CA) are after Miyashiro (1973). Symbols as in figure 6.

are surrounded by serpentinitic melange and basalts with N-MORB characteristics (Fig. 3; Buslov et al., 1993; Gibsher et al., 1996).

Two types of Vendian-Early Cambrian volcanic rocks occur in the Katun paleo-island: (a) thin flows of tholeiitic basalts – the relicts of oceanic crust – formed in a deep-water setting; and (b) large volcanic edifices and submarine plateaux of alkali basalts and subordinate tholeiites. The first type are aphyric tholeiites with sporadic micro-phenocrysts of olivine and clinopyroxene. The second type are aphyric olivine-bearing tholeiites, porphyritic olivine hawaiites, and aphyric or plagioclase-porphyritic alkali basalts consisting of olivine, pyroxene and plagioclase phenocrysts in a glassy matrix (Buslov et al., 1993; Gibsher et al., 1996).

The Katun accretionary wedge is overlain by basal conglomerates of the Shashkunar Formation. This formation is dominated by carbonate rocks and is the stratigraphically lowest member of the Early-Middle Cambrian island arc sequence. The tectonic sheets of the accretionary wedge and the carbonate rocks of the Shashkunar Formation are cross-cut by island-arc dykes of pyroxene-plagioclase porphyrites, diabase and gabbro.

Biostratigraphy

The rocks of the Katun paleo-oceanic island contain abundant remnants of microphytoliths, calcareous algae and sponge spicules indicating a Late Vendian to Early Cambrian age (Terleev, 1991).

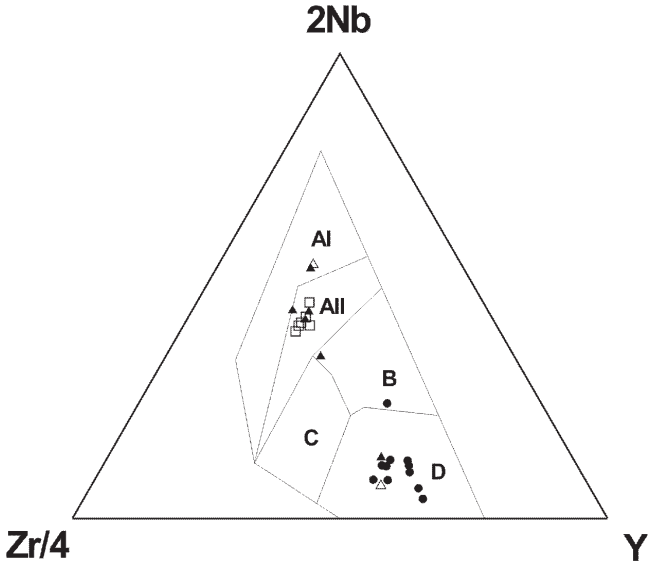

Fig. 8. The Zr/4-2Nb-Y discrimination diagram after Meschede (1986). The fields are defined as follows: AI, within-plate alkali basalts; AII, within-plate alkali basalts and within-plate tholeiites; B, E-type MORB; C, within-plate tholeiites and volcanic-arc-basalts; D, N-type MORB and volcanic-arc basalts. Symbols as in figure 6.

Three localities at Edigan, Elandin and Cheposh are the best examples of the structure and rock assemblages of the Katun paleo-oceanic island.

The Edigan site (Fig. 3) is located on the right bank of the Katun River. The Edigan monocline is composed of paleo-oceanic island rocks. Associated Late Vendian-Early Cambrian cherts, sandstones, mudstones and limestones of the Eskongin Formation represent slope facies of the paleo-oceanic island, and volcanic rocks of the Manzherok Formation, constitute an oceanic island bottom facies and an upper facies of reef limestones. Sponge spicules, calcareous algae and small shelly fossils from terrigenous and carbonate rocks of the Eskongin Formation are Lower Cambrian in age (Terleev et al., 2002). Dolomites overlapping volcanic rocks of the Manzherok Formation contain Late Vendian-Early Cambrian stromatoliths and microphytoliths (*Nubecularites punctatus* and *N. catagraphus*) and alga (*Girvanella* sp.) (Terleev, 1991).

The total thickness of the section is 3000 m. The Eskongin Formation conformably overlies volcanic rocks of the Manzherok Formation, the basaltic sequence which reaches a thickness of more than 2500 m.

The Elandin site is located on the right bank of the Katun River (Fig. 3). Of special interest are Late Vendian-Early Cambrian reef dolomites, which we suggest were formed on top of a paleo-oceanic island. The dolomites overlie volcanic rocks of the Manzherok Formation. The light-gray to gray massive and clastic dolomites have a thickness of 250 m, and contain stromatoliths and microphytoliths. The microphytoliths include *Nubecularites punctatus* Reitl., *N. catagraphus* Reitl., *Osagia* sp., *Vesicularites flexuosus* Reitl., *Ves. lobatus* Teirl., *Ves. bothrydiophormis (Krasn.), Ves. reticulatus Varizh., Ves. igaricus Milstein, Ves. compositus* Z. Zhur., *Ves. pussilus* Zabr., *Nubecularites uniformis* Z. Zhur., *Ambigolamellatus horridus* Z. Zhur., *Radiosus sphaericus* Z. Zhur., *Volvatella vadosa* Z. Zhur., *Glebosites gentilis* Z. Zhur., *osagia tenuilamellata* Reitl., *Vesicularites textus* Klinger. Microphytoliths *Nubecularites punctatus* and *N. catagraphus* and alga *Girvanella* sp. indicate a Late Vendian-Early Cambrian age for the dolomites (Terleev, 2002).

The Cheposh site is located in the Katun valley, near Cheposh Village (Fig. 3). There, tectonic sheets composed of paleo-oceanic island rocks alternate with two types of deformed olistostrome. The accretionary wedge is unconformably overlain by the basal conglomerates and Early Cambrian–Middle Cambrian andesitic basalts, volcaniclastic rocks and limestones of a normal island arc (Buslov et al., 1993). The Early-Middle Cambrian age (Botomian-Amgian) of the island arc comprising limestones, volcaniclastic and volcanic rocks is established by numerous discoveries of archaeocyathean and trilobites (Repina and Romanenko, 1964; Buslov et al., 1993).

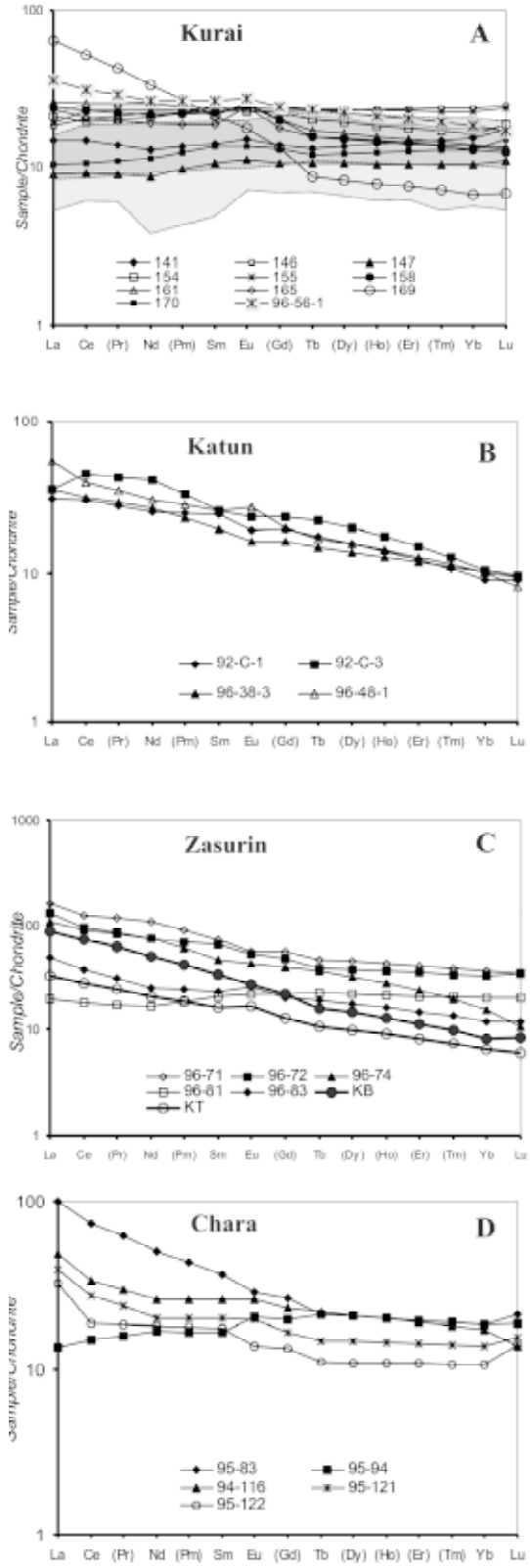

Fig. 9. Chondrite-normalized rare-earth –element (REE) plots for (A) Kurai, (B) Katun, (C) Zasurin and (D) Chara metavolcanic rocks. The gray and light gray fields in (A) are Nauru and Ontong Java OPB, respectively. The normalizing values are from McDonough and Sun (1995).

Table 2. Major and trace element analyses of metabasalt rocks from the Katun accretionary wedge.

Sample	92-C-1	92-C-3	96-38-3	96-48-1
SiO_2	52.32	47.62	42.26	46.94
TiO_2	2.26	2.4	1.51	3.07
Al_2O_3	12.44	13.04	14.79	13.79
Fe_2O_3	11.11	13.85	9.40	12.17
MnO	0.1	0.14	0.23	0.16
MgO	6.19	7.42	6.94	5.26
CaO	7.6	8.81	13.59	9.86
Na_2O	5.04	3.7	3.95	2.36
K_2O	0.68	0.41	0.46	1.55
P_2O_5	0.29	0.31	0.17	0.28
L.O.I.	2.76	3.42	6.98	4.76
Total	99.78	99.86	100.27	100.22
La	9.5	11	11	17
Ce	24.5	36	25	32
Nd	15	24.5	16	18
Sm	4.7	5	3.8	5
Eu	1.4	1.72	1.2	2
Gd		5.2		4
Tb	0.82	1.05	0.7	0.8
Yb	1.9	2.2	2.1	2.1
Lu	0.29	0.31	0.3	0.26
Sc	23.6	23	39	30
Th	0.6	0.6	0.9	1.5
Hf			2.1	4
Ta	1.1	1.2	0.9	1.4
Ba			95	350
Co			40	56
Cr			100	100
Rb	6.5	2.56	5	25
Sr	120.4	267.8	300	800
Y	23.9	18.7	13	27
Zr	140.8	124.4	80	170
Nb	20.5	17.7	14	26
Zr/Nb	6.87	7.03	5.71	6.54
(Nb/La)N	1.19	1.41	0.70	0.85
(La/Ta)N	0.97	0.65	0.87	0.86
(La/Yb)N	3.37	3.37	3.53	5.46

Major elements are in wt.% and trace elements in ppm. Sample 96-48-1 is a basalt pebble from the basal conglomerate overlapping oceanic island units.

Geochemistry of basaltic rocks

Whole-rock analyses of four selected metabasaltic rocks from the Katun accretionary wedge are given in table 2. The Katun basalts belong to the low-temperature greenschist facies of regional metamorphism and probably experienced sea-floor metamorphism, although meso- and microscopically they look less altered than the Kurai metabasalts. The pillows are highly altered, and consist of Cpx-porphyritic basalt cemented by inter-pillow siliceous-carbonate sediments. Pyroxene is replaced by chlorite and epidote and the matrix comprises actinolite, epidote, chlorite and albite. The Katun metabasalt rocks are mainly classified as alkaline basalts (Fig. 6). Katun samples have Ti contents close to the Kurai samples and FeO*/MgO ratios ranging mostly from 1.25 to 2.1, which show a medium degree of differentiation (Table 1).

TiO_2 and P_2O_5 contents range from 1.52 to 3.07 wt.% and from 0.17 to 0.31 wt.%, respectively. Al_2O_3 ranges from 12.4 wt.% to 14.8 wt.%, that is in average a little lower than in IAT. Similar to the Kurai metabasalts, the Katun mafic volcanic rocks are slightly depleted in LILE (possibly due to the alteration) and enriched in HFSE, Cr and Mg compared to IAT (Table 2; Frolova and Burikova, 1997).

The samples have Zr/Nb ratios below 20, intermediate Nb/Zr (0.14–0.18) and Nb/Y bulk ratios (0.86–1.08) suggesting their OIB origin (Table 2). In the Nb-Zr/4-Y diagram the samples plot in the within-plate alkali basalt field (Fig. 8).

REE patterns show obvious LREE enrichment (Fig. 9) with La_N = 30–54, $(La/Yb)_N$ = 3.3–5.4. Most samples lack Eu anomalies. MORB-normalized trace element patterns show that Y, Sc and Cr are more depleted than MORB but other HFSE are enriched (Fig. 10B). LILE in all samples is higher than in MORB due to the OIB alkaline nature of the Katun samples and their probable secondary alteration. No Nb-Ta and Ti depletions have been found, and the contents of those trace elements are close to those of the Honolulu volcanics of Hawaii (Clague and Frey, 1982). In chondrite-normalized spidergrams (Fig. 11) the Katun metabasalts display mild Nb-Ta enrichments relative to La (i.e., $Nb/La_N > 1$). Thus, the Katun metabasalts resemble many oceanic alkali basalts formed without crustal contamination. Nb/Y and Nb/Zr ratios of the basalts plot in the field of Hawaiian hotspot (Fig. 12A). In the Ti/Yb versus Nb/Th plot the samples also lie close to the field of Hawaiian OIB (Li et al., 2002) (Fig. 12B).

The data indicate that the Katun metabasalts represent an OIB series, which possibly formed within an oceanic island environment related to hot spots.

Charysh-Terekta Strike-slip Zone: Late Cambrian-Early Ordovician Oceanic Crust

Structural position

The Charysh-Terekta strike-slip zone in NW Altai (Fig. 1) extends over a distance of 120–130 km and consists of five deformed structural units (from west to east): Inya, Kur'ya-Akimov, Charysh, Zasurin, and Talitsa. They occur as structural sheets and lenses bounded by the late Carboniferous-Permian North-Eastern and Bashchelak faults (Fig. 4). These units are composed of sandstones, cherts, pillow-basalts, volcanoclastics, and gabbro-diabase sills and dykes (Buslov et al., 2000).

Of special interest is the Zasurin Formation (or terrane) (Fig. 4), which comprises several tectonic lenses consisting of multi-colored sandstones and cherts, variolitic or aphyric pillow-lavas, plagioclase and pyroxene-plagioclase

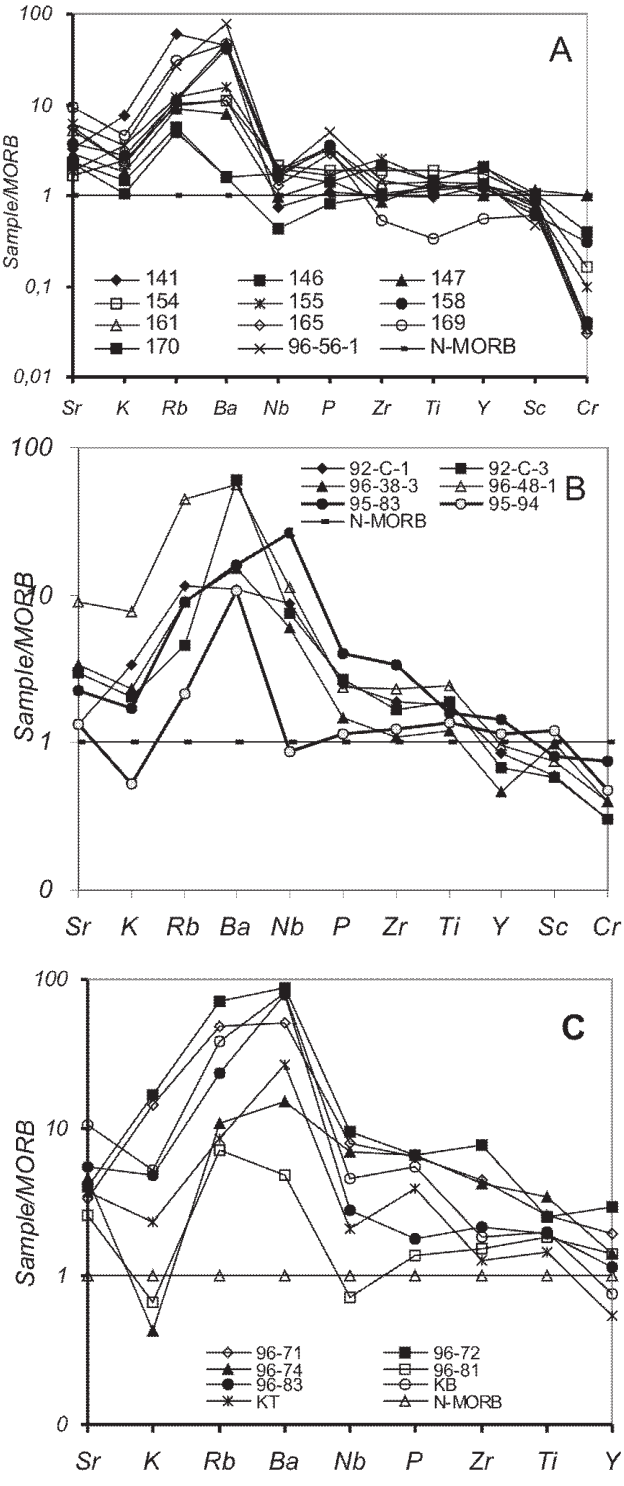

Fig. 10. MORB-normalized trace element patterns for (A) Kurai, (B) Katun and Chara (bold lines), and (C) Zasurin metavolcanic rocks. Normal-type mid-ocean ridge basalt normalizing values are from Sun and McDonough (1989).

basalts and their volcaniclastic derivatives, gabbro and gabbro-diabase sills and dykes. Sennikov et al. (2003) considered four lithological types in the Zasurin

Formation: (1) basalt-chert-sandstone, (2) chert, (3) chert-sandstone, and (4) sandstone-mudstone types. The breccia, co-sedimentation and Z-shape folding textural features of the cherts suggest that they represent slope facies of oceanic islands. The Zasurin Formation is characterized by a unique combination of terrigenous, volcanic and siliceous units. The color of the cherts ranges from red and brown to violet, which is typical of present-day seamount slope sedimentation environments. Siliceous rocks are evenly distributed throughout the section. The thickness of the silica-rich packages reaches several hundred meters, and individual siliceous beds reach thicknesses of 20–30 meters.

Biostratigraphy

Biostratigraphic and structural data show that the Zasurin Formation consists of three suites. The lower suite comprises red and gray sandstone-mudstone strata, gray cherts, and basaltic rocks. The middle suite consists of gray sandstones and siltstones. The upper suite comprises alternating red and gray strata of sandstones and cherts and interbeds of tuffs and tuff-sandstones (Sennikov et al., 2003). The stratified dark-red and gray-green cherts of the Zasurin Formation contain various Late Cambrian-Early Ordovician (Late Tremadoc-Early Arenig) pelagic planktonic conodonts, radiolarians with siliceous skeletons and benthonic sponge spicules (Iwata et al., 1997b; Sennikov et al., 2003). Both benthic and planktonic pelagic radiolarian faunae are much poorer than those of the planktonic pelagic conodonts (typically over 10 taxa). In spite of their poor faunae, both benthic and pelagic radiolarians occur in large numbers. In contrast, although more than ten taxons of conodonts occur, the number of their specimens present is only moderate.

The age of the Zasurin units is determined based on the conodont biostratigraphic zonation of Sennikov et al. (2003): (1) Aksai stage, *W. matsushitai* and *M. erectus* zones; (2) Batyrbai stage, *P. mueleri*, *E. notchpeakensis*, and *C. Minutus* zones; (3) Tremadoc-Arenig boundary, *P. proteus* zone, and (4) Lower-Middle Arenig, *P. elegans* and *O. evae* zones. Thus, the oceanic basalt-siliceous-terrigenous deposits of the Zasurin Formation were formed in the Aksai, Batyrbai, Tremadoc and Arenig stages (Sennikov et al., 2003).

Geochemistry of basaltic rocks

Whole-rock analyses of the basaltic rocks of the Zasurin Formation were reported by Buslov et al. (1999, 2000, 2001). The major-element compositions listed in table 3 include 10 previously published analyses (Buslov et al., 2000, 2001) and three new analyses. This major element chemistry forms the foundation for our trace element study of these basalts. The analyses are listed as analyzed, with Fe tabulated as Fe_2O_3. Most of the analyzed basalts are altered, with phenocrysts and groundmass replaced by saussurite, chlorite, calcite, and magnetite. Most samples contain more than 2 wt.% H_2O (based on LOI), and the compositions of these samples may have been slightly modified by late-stage alteration. It seems that Mg, Fe, Ca and alkalis show considerable variations from one rock to another, whereas Ti and Al remain rather constant, despite processes of sea-floor weathering and metamorphism. More or less fresh basalts (samples G-2921, E-2921, 96-86-20, 96-C-3, 96-81, 97-120-1) have low K_2O, TiO_2 and P_2O_5 values. MgO, CaO, Al_2O_3 and SiO_2 contents are less diagnostic but are still in accordance with those recorded in tholeiitic oceanic basalts. P_2O_5 and TiO_2 seem to have diagnostic value for the identification of the tholeiitic parentage of the Zasurin samples. Samples 95-130, 96-71, 96-72, 96-74, 97-120-5 and B-2921 have TiO_2 contents exceeding 2.5 wt.% and P_2O_5 values are mostly greater than 0.4 wt.%. As shown by the Nb/Y ratios, one sample is subalkaline basalt and the rest are alkaline basalts (Fig. 6). Samples KB and KT (respectively) are those of Kaula basanite and tholeiite (Hawaiian Islands) given for comparison (Clague and Frey, 1982; Garcia et al., 1986).

Trace elements were determined for five samples (Table 4). TiO_2 and P_2O_5-rich samples are enriched in HFSE (Zr, Hf, Nb, Ta, Y) and some also contain increased contents of LILE (K, Rb, Ba, Sr) and LREE. Nb/Zr ratios range from 0.04 (96-81) to 0.15 (96-74) and plot in the field of the Hawaiian hot spot (Fig. 12A). In the Nb-Zr/4-Y diagram, sample 96-81 plots in the field of N-MORB, sample 96-83 plots between P-MORB and within-plate alkali basalts and tholeiites, and all other samples plot in the field of within-plate basalts (Fig. 8). Thus, according to major element concentrations, we recognize two groups of samples: (1) samples with low TiO_2, P_2O_5 and alkalis, which seem to possess MORB characteristics (96-81, 96-C-3, 97-120-1 and G-2921) and (2) samples with opposite features, having OIB affinities (96-83, 95-130, 96-71, 96-72, 96-74, 97-120-5, B-2921 and E-2921). Sample 96-82-20 seems to be intermediate between these groups.

The OIB-type samples show obvious LREE enrichment with La_N = 106–160, $(La/Yb)_N$ = 3.9–6.9 and are thus close to the Kaula basanite. The MORB-like sample (96-81) possesses smaller LREE enrichment with La_N = 19, $(La/Yb)_N$ = 0.96 (Fig. 9). It is distinguished from the Kaula tholeiite by HREE depletion, and also differs from modern N-MORB in lacking LREE-depletion. Thus, the REE pattern of sample 96-81 resembles T-MORB or OPB. No samples show Eu anomalies. MORB-normalized trace element patterns show that HFSE and LILE are more enriched than MORB (Fig. 10). These patterns also resemble those of

oceanic plateau basalts (Saunders, 1986) in showing enrichment in almost all incompatible elements relative to N-MORB. Most samples have similar patterns resembling so-called transitional MORB (T-MORB) (Ueda et al., 2000). No Zasurin samples have very low HFSE. The group of samples with MORB affinities display weak depletion in Nb (i.e., $Nb/La_N < 1$) whereas the second group are enriched (Nb/La_N ranging between 1.03 and 1.44) (Table 4). Because most rocks display no Nb or Ti negative anomalies we suggest that they were formed not

Table 3. Major element analyses of metabasalt rocks from the Zasurin Formation.

Sample	95-130	96-71	96-72	96-74	96-81	96-83	96-C-3	96-86-20	97-120-1	97-120-5	B-2921	G-2921	E-2921	KB	KT
SiO_2	46.4	49.05	52.37	48.10	48.15	46.44	49.92	45.51	48.93	45.91	46.56	47.93	48.2	46.65	47.60
TiO_2	2.39	2.73	2.71	3.46	1.96	2.04	0.50	1.04	1.32	2.79	3.19	1.56	1.99	2.13	1.59
Al_2O_3	18.75	14.08	14.7	13.97	13.78	14.36	20.00	13.54	13.74	15.3	19.49	13.72	16.1	14.71	15.10
Fe_2O_3	8.46	16.87	15.37	11.96	14.15	12.44	8.81	8.22	9.68	13.19	14.16	13.89	12.14	11.33	13.41
MnO	0.11	0.08	0.14	0.28	0.26	0.22	0.17	0.19	0.2	0.18	0.15	0.21	0.2	0.16	0.12
MgO	5.5	2.49	1.97	5.90	6.99	8.57	2.92	4.72	8.35	7.72	2.29	7.45	6.79	8.61	5.40
CaO	8.8	4.70	4.25	6.12	10.91	8.20	10.53	11.88	9.66	8.11	3.18	9.77	8.08	9.96	11.49
Na_2O	2.85	4.89	3.15	3.79	2.14	2.85	3.06	2.15	2.46	2.5	2.14	2.27	2.73	3.70	2.39
K_2O	0.65	2.82	3.25	0.08	0.13	0.92	0.08	0.46	0.41	0.36	5.37	0.24	0.76	1.03	0.45
P_2O_5	0.61	0.72	0.75	0.72	0.16	0.20	0.09	0.33	0.18	0.38	0.57	0.16	0.27	0.62	0.44
L.O.I.	4.92	1.94	1.35	5.62	2.7	3.44	3.77	1.49	5.06	3.49	2.83	2.77	2.77	1.57	2.04
Total	99.44	100.38	100.01	100	101.34	99.67	99.85	99.96	99.99	99.93	99.93	99.97	100.03	100.47	100.03

New analyses as distinct from previously published data are as follows: 96-74, 96-81, B-2921, G-2921, E-2921

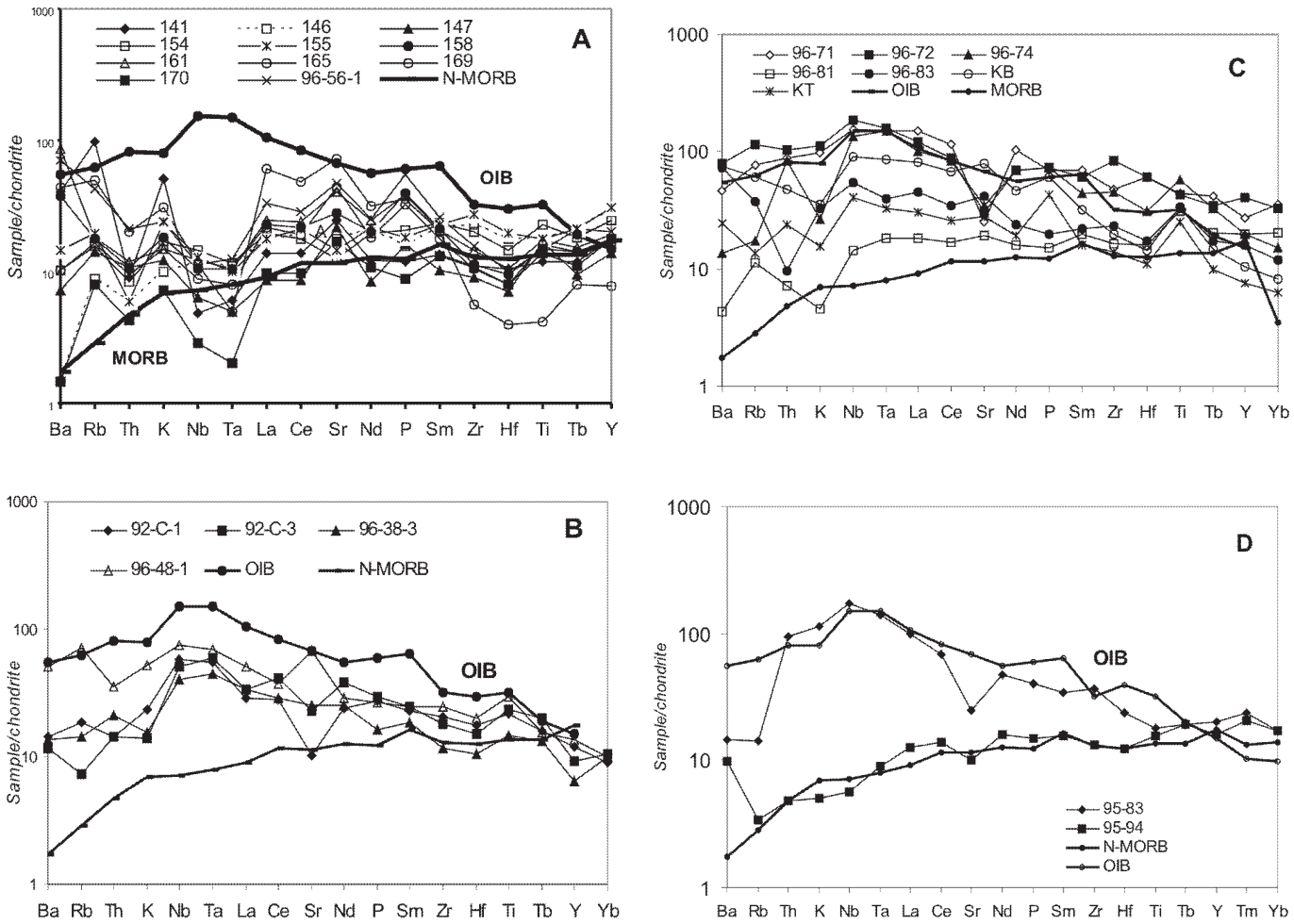

Fig. 11. Chondrite-normalized multi-element diagrams for (A) Kurai, (B) Katun, (C) Zasurin and (D) Chara metavolcanic rocks. The normalizing values are from Sun and McDonough (1989).

by fractional crystallization, but by partial melting of a rather deep enriched mantle source.

The chondrite-normalized spidergrams (Fig. 11) of Zasurin basaltic rocks are intermediate between OIB (OIA) and N-MORB. Samples 96-71, 96-72, 96-74 display enriched patterns overall, except for depletion in Sr, possibly due to sea-floor alteration. The patterns of 96-71 and 96-72 are closest to OIB, whereas 96-81 resembles MORB. The rest generally range between OIT (KT) and typical OIA.

In the Nb/Zr versus Nb/Y diagram, sample 96-81 plots in the field of MORB, and the second group of samples plots in the field of Hawaii OIB, i.e. normal hotspot (Fig. 12A) (Tatsumi et al., 1998). In the Ti/Yb versus Nb/Th plot (Fig. 12B) KB, KT and all the Zasurin samples except for 96-83 and 96-74 have very uniform Nb/Th (15.3±1.1) ratios close to that of OIB. The Ti/Yb ratios are however lower than those of Hawaiian OIB according to OIB data from Feigenson et al. (1996) and Hofmann and Jochum (1996), due to the higher Yb contents (Table 4). They could be formed by the mixing of OIB-sources with mafic oceanic crust material. These tendencies are in accord with the above discrimination of the samples between OIT and OIA, except for 96-81, which is similar to OPB or T-MORB.

Chara Ophiolitic Strike-slip Zone: Late Devonian-Early Carboniferous Oceanic Crust

Structural position

The Chara ophiolitic belt (Fig. 5) is a main collisional zone located along the northeastern margin of the Kazakhstan continent. This north-west trending belt occupies an area 20–30 km wide and 100 km long, and extends along the Irtysh Shear Zone (Fig. 1). It was formed in the Middle-Late Paleozoic, and consists of several allochthonous structural units. The Chara belt comprises three types of serpentine mélanges including dismembered ophiolites, volcanic rocks, high-pressure metamorphic rocks, olistostromes, limestones, and cherts.

The Early Paleozoic subduction mélange is situated in the southeastern Chara zone. The high-pressure metamorphic rocks are meta-gabbro and meta-basalt, metamorphosed deep-water siliceous sediments, eclogites, amphibolites and glaucophane schists.

The Ordovician ophiolitic mélange contains blocks of oceanic basaltic lavas and layers of siliceous mudstone and chert.

The Late Carboniferous-Early Permian mélange separates tectonic sheets that were brought to the fault zone from the margins of Siberian and Kazakhstan continents. The mélange usually has a NW orientation and coincides with the strike of the Chara fault zone. The blocks within the mélange are also oriented in this direction. The blocks are variable in composition, and include rocks from both the subduction and ophiolite tectonic units (Fig. 5).

The following three stages have been distinguished in the evolution of the Chara ophiolite belt and adjacent island arcs (Buslov et al., 2003):

(1) Subduction of the Paleo-Asian Ocean crust and formation of the accretionary prism occurred during Late Devonian-Carboniferous time (Visean-Namurian).

(2) Collision of the Siberian and Kazakhstan continents resulted in large-scale faulting in Middle Carboniferous and Early Permian time.

(3) Permian post-collisional magmatism and faulting.

Biostratigraphy

Chert samples with microfossils were collected in the southern part of the Chara ophiolite belt. The Urumbaev Formation consists of rhythmic siltstones, reef and bedded limestones, and cherts with thin intercalations of terrigenous sandstone, frequently accompanied by manganese ores. Rock colors vary from violet to dark gray. The Urumbaev Formation is considered to have been deposited on the slopes of paleoseamounts (Iwata et al., 1997a). Light-brown cherts yielded the following radiolarians: *Archocyrtium* cf. *typicum* Cheng, *Tetrentactia barysphaera* Foreman, *Entactinosphaera* cf. *echinata* Foreman, *Astroentactinia stellata* Nazarov, *Astroentactinia* aff.

Table 4. Trace element analyses of metabasalt rocks from the Zasurin Formation.

Sample	96-71	96-72	96-74	96-81	96-83	KB	KT
La	50	40	33	6	15	27.1	10
Ce	100	76	72	14.5	30	59	22.3
Nd	65	44	44	10	15	29.7	12.3
Sm	14	12.5	9	4	4.5	6.48	3.21
Eu	4.1	3.8	3.1	1.6	1.9	2	1.24
Tb	2.2	1.8	1.7	1.05	0.9	0.76	0.51
Yb	7.5	6.8	3.2	4.2	2.5	1.7	1.33
Lu	1.1	1.1	0.34	0.64	0.38	0.27	0.19
Sc	38	35	29	57	48		
Th	3.7	4.3	3.5	0.3	0.4	2	1
Hf	12	12	6.2	3.2	3.5	2.9	2.2
Ta	3	3.2	3	0.37	0.8	1.7	0.65
Ba	320	550	95	30	500	513	169
Co	26	28	30	52	53		
Cr	78	53	48	100	93		
Rb	27	40	6	4	13	21.3	4.8
Sr	300	360	408	230	490	938	330
Y	54	82	40	40	32	21	15
Zr	330	565	310	112	160	136	95
Nb	54	65	47	5	19	31.6	14.3
Zr/Nb	6.11	8.69	6.60	22.40	8.42	4.30	6.64
(Nb/La)N	0.96	1.44	1.26	0.74	1.12	1.03	1.27
(La/Ta)N	1.08	0.81	0.71	1.05	1.21	1.03	0.99
(La/Yb)N	4.49	3.97	6.95	0.96	4.05	10.75	5.07

paronae, *Entactinia* sp., *Helioentactinia prismaspinosa* Wakamatsu, and others (Iwata et al., 1994, 1997a). The radiolarian assemblages described suggest that the Urumbaev Formation is Late Devonian (Fammenian). The limestones contain Upper Devonian climeniides and goniatites (Sennikov et al., 2003).

The Karabaev Formation consists of pillow-lavas, siliceous mudstones and cherts. The green-gray, gray, violet and red siliceous rocks are possibly fragments of ophiolites. Late Devonian conodonts were recovered from the stratified cherts overlying basalts. Besides conodonts, the red cherts contain abundant Tournaisian radiolarians, but most skeletons have been dissolved (Sennikov et al., 2003).

The Verachar Formation consists of basaltic, basaltic-andesite, and andesites, tuffaceous sandstones, clay-siliceous mudstones, cherts, and limestones. Siliceous rocks are gray, gray-green and red. This formation was deposited in a marginal basin setting adjacent to an island arc. Gray chert of the Verachar Formation yielded the following radiolarians: *Albaillella* cf. *papadoxa* Deflandre and *Polyentactinia* sp., therefore the age of these cherts is considered to be Earliest Carboniferous (Tournaisian) (Iwata et al., 1997a). The Visean age of the Verachar Formation was also suggested based on the Givetian-Franian fauna in the limestones (Sennikov et al., 2003).

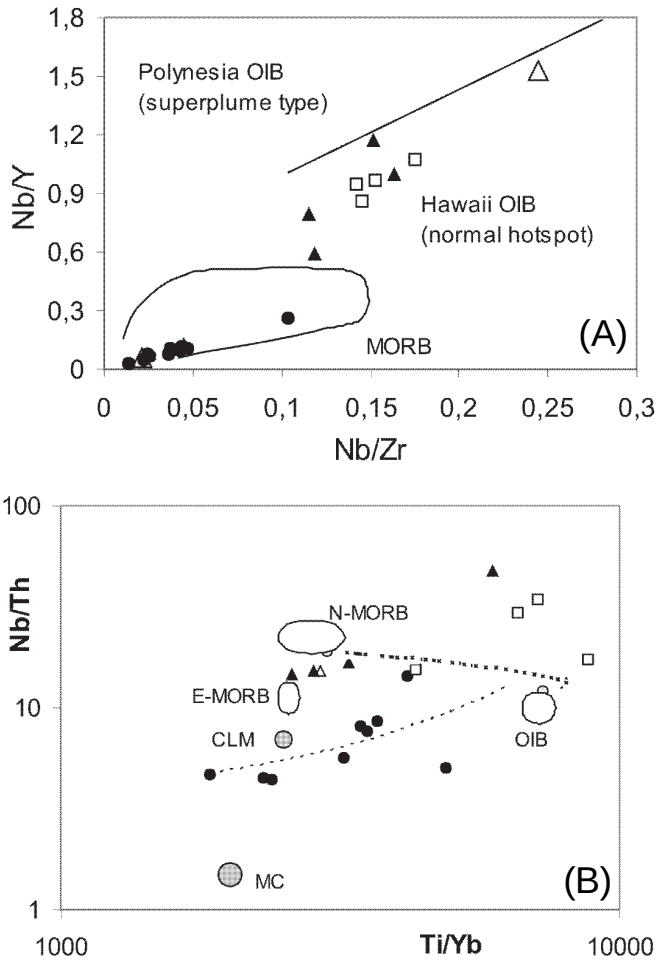

Fig. 12. Nb/Zr vs Nb/Y (A) and Ti/Yb vs Nb/Th (B) plots for Kurai, Katun, Zasurin and Chara volcanic rocks. The data for OIB and MORB are after Sun and McDonough (1989), and those for middle crust (MC) and continental lithosphere mantle (CLM) from Li et al. (2002). Symbols as in figure 6.

Geochemistry of basalts

The basaltic rocks under investigation were sampled from the Type 2 and Type 3 mélanges and the Urumbaev and Verochar Formations. They include porphyritic basalts, dolerite, amygdaloidal basalt, basaltic andesite, andesite and their tuffs and spilite. Subophitic to intersertal, porphyritic and doleritic textures predominate, although some samples are aphyric. Some samples contain a few modal percent of euhedral to subhedral clinopyroxene (augite?) phenocrysts, rarely larger than 0.5 mm, and albitized plagioclase phenocrysts are more abundant. Less frequently, calcic plagioclase is preserved in some basalts, but it is generally altered to albite or very fine-grained aggregates of pumpellyite and chlorite. Primary Fe-Ti-oxides occur almost exclusively as a groundmass phase. The groundmass consists of plagioclase laths, clinopyroxene, and magnetite. Glassy groundmass in most crystalline basalts is replaced by pleochroic green chlorite, minor pumpellyite, epidote, chalcedony and Fe-hydroxides. Thin veinlets of prehnite, quartz and calcite intersect the rocks but constitute less than 0.1 per cent of the rock mass. Some amygdules are filled by prehnite, quartz and calcite. The secondary mineral assemblages correspond to the prehnite-pumpellyite and greenschist facies of metamorphism.

Whole-rock analyses of tholeiitic, alkaline and andesitic basalts from the Chara ophiolitic belt are given in table 5.

Most fresh basalts (samples B-95-94, 97-116, 97-117, 97-118) have low alkali contents, and low K_2O, TiO_2 and P_2O_5 values are particularly notable. These chemical features are typical of oceanic ridge tholeiites (Kay et al., 1970). The other samples have rather high contents of these elements: TiO_2 contents range from 1.2 to 2.6 wt.% and P_2O_5 from 0.13 to 0.57 wt.% (Table 5). On average, these concentrations are higher than those in metabasalts from the Kurai and Katun accretionary wedges, although they are within the same range of values. K_2O and Na_2O are enriched in all altered and recrystallized samples, whereas MgO contents are depleted in the same rocks. MnO content remains quite constant in all analyzed samples but there is a tendency for CaO to decrease with increasing SiO_2. Most samples are intermediate between sub-alkalic and alkalic basalts (Table 5). The Chara rocks display moderate Fe-enrichment trend with advancing

fractionation (Fig. 7A). However, TiO_2 does not clearly increase with increasing FeO*/MgO, suggesting character intermediate between abyssal tholeiite and island-arc tholeiite (Fig. 7B). The FeO* vs FeO*/MgO trend allows the conclusion that the range of tholeiites (left branch in Fig. 7A) in the Chara ophiolite belt was produced by advanced fractionation of one or more tholeiitic parent magmas. FeO*/MgO ratios show two ranges: 1–2.5 and 3.5–6, with tholeiitic and calc-alkaline affinities respectively (Fig. 7). For the mafic samples, TiO_2 and MgO increase and Al_2O_3 decreases with increasing SiO_2, in contrast to the andesitic rocks which have opposite tendencies. It is noteworthy that all the mafic samples have high LOI (1.96 to 8.76%) indicating moderate to strong alteration. Because Na, K and LILE are mostly mobile, only the HFSE and REE are used in the following discussion.

Overall, the basalts range from evolved to differentiated compositions with Mg# between 0.46 and 0.30. The andesites have lower Mg# of 0.34–0.15. However, Mg and Fe are susceptible to change during alteration, and we do not use these values for interpretation. According to P_2O_5/TiO_2 ratio, reflecting degree of enrichment in incompatible elements (Mullen, 1983; Rhodes, 1973), we distinguish two groups of samples: those with MORB and OIT affinities, having $P_2O_5/TiO_2<0.15$ (samples 95-94, 95-121, 95-122, 97-116, 97-117, 97-118, 97-119-3); and those with OIA affinities (samples 95-83, 95-116, 97-102, 97-103-2, 97-104, 97-105, 97-107, 97-108, 97-111) (Table 5).

A complete set of trace elements was determined in two samples (95-83 and 95-94), and REE and several HFSE were determined in three other samples (94-116, 95-121 and 95-122) (Table 6). High-Ti and high-P greenstones contain increased contents of HFSE and some LILE (La, Ce, Rb, Ba, Sr). Sr and Ba could have been captured from seawater following eruption on the sea floor. Cr contents are variable, ranging from 15 to 185 ppm, whereas Sc contents remain quite constant and close to that of Kurai, Katun and Zasurin greenstones (Tables 1, 2, and 4). High Nb indicates that sample 95-83 probably has an OIB affinity, whereas sample 95-94 is closer to MORB. In the Nb-Zr/4-Y diagram, sample 95-94 plots in the field of N-MORB, and sample 95-83 plots in the field of within-plate basalts (Fig. 8).

REE were determined in five samples (Table 6, Fig. 9d). OIB sample 95-83 has a REE pattern showing obvious LREE enrichment with $La_N = 106$, $(La/Yb)_N = 5.85$, and is similar to OIB samples from the Zasurin Formation. It also has a negative Eu anomaly, suggesting plagioclase fractionation from the melt. Sample 95-94 (MORB affinity) possesses no LREE enrichment with $La_N = 13.5$, $(La/Yb)_N = 0.75$, and is similar to Zasurin MORB greenstones. Samples 94-116, 95-121 and 95-122 have intermediate LREE with $La_N = 32–48$, $(La/Yb)_N = 1.01–3.06$ and are close to Katun greenstones (Tables 2 and 6, Fig. 9D).

MORB-normalized multi-element patterns show HFSE concentrations close to MORB in two samples, although in OIB sample (95-83) they are higher (Fig. 10B). Unlike the samples discussed above, the Chara greenstones show no HFSE depletions. MORB sample (95-94) has a weak negative Nb anomaly. In the chondrite-normalized spidergrams (Fig. 11D) the basalt of OIB type displays mild Nb-Ta enrichment relative to La ($Nb/La_N = 1.64$), unlike the MORB sample, which is clearly depleted in Nb-Ta ($Nb/La_N = 0.42$). The OIB sample shows a weak enrichment in Th but depletion in Hf, so we cannot suggest crustal contamination. Both samples have negative Sr anomalies, suggesting plagioclase precipitation.

Thus, we may distinguish three groups of basaltic rocks in the Chara belt: basaltic andesite basalt, basalts with

Table 5. Major element analyses of metabasaltic rocks from the Chara belt.

	AB	TH	And	AB	TH	TH	And	TH	TH	And	AB	AB	AB	AB	AB	AB	BTA
	1	2	3	4	5	6	7	8	9	10	11	12	13	14	15	16	17
Sample	95-83	95-94	95-113	95-116	95-121	95-122	97-102	97-103-2	97-104	97-105	97-107	97-108	97-111	97-116	97-117	97-118	97-119-3
SiO_2	46.37	48.52	53.81	43.10	44.69	43.84	52.77	48.37	46.52	54.33	47.79	46.63	51.66	49.28	49.67	48.17	50.38
TiO_2	1.85	1.61	1.92	2.65	1.43	1.40	1.61	1.52	2.04	1.28	2.64	2.55	2.13	2.43	2.39	2.45	2.67
Al_2O_3	16.47	12.75	18.00	14.17	19.75	20.08	16.35	15.36	17.70	16.90	16.11	15.16	17.95	13.16	11.65	12.63	15.68
Fe_2O_3	7.83	11.51	9.34	11.84	5.63	4.96	12.07	10.59	11.36	9.61	11.65	12.65	11.73	15.04	14.83	15.23	9.85
MnO	0.18	0.21	0.15	0.12	0.20	0.16	0.20	0.14	0.16	0.20	0.15	0.16	0.17	0.21	0.20	0.19	0.17
MgO	4.93	6.48	1.43	4.60	4.34	4.29	2.28	5.07	4.34	4.50	5.05	5.48	2.75	6.70	7.33	6.66	2.54
CaO	8.87	12.40	2.47	8.30	8.05	8.88	4.55	9.97	9.25	4.57	5.91	6.70	5.40	6.80	8.90	9.09	9.36
Na_2O	5.58	2.68	7.35	3.55	2.31	2.40	4.60	1.89	2.22	5.62	3.87	4.03	3.34	3.05	2.51	2.05	3.33
K_2O	0.32	0.10	2.16	2.25	4.94	4.58	0.68	0.21	0.23	0.19	1.00	0.45	1.85	0.37	0.31	1.21	1.40
P_2O_5	0.43	0.13	0.57	0.36	0.17	0.14	0.84	0.25	0.35	0.28	0.37	0.36	0.63	0.25	0.21	0.22	0.36
LOI	7.34	3.58	2.38	9.03	8.76	9.33	4.02	6.80	5.91	2.44	5.42	5.92	2.39	2.75	1.96	2.21	4.23
Total	100.17	99.96	99.57	99.97	100.26	100.06	99.97	100.17	100.08	99.92	99.96	100.09	100.00	100.04	99.96	100.11	99.97
P_2O_5/TiO_2	0.23	0.08	0.3	0.14	0.11	0.1	0.52	0.16	0.17	0.22	0.14	0.14	0.29	0.1	0.09	0.09	0.13

Note: Sampling locations (Fig. 5) – 1–Nikolaevka; 2–Akzhal; 3–Georgievka; 4-6, 17–Igorevka; 7-14–Charsk; 15-16–Zhangiz-Tobe
AB–alkaline basalt, TH–tholeiitic basalt, And–andesite, BTA–basaltic trachyandesite.

Table 6. Trace element analyses of selective volcanic rocks of the Chara belt.

	95-83	95-94	Б-94-116	Б-95-121	Б-95-122
La	33	4.2	15	12	10
Ce	60	12	27	22	15
Nd	30	10	15.5		
Sm	7	3.2	5	3.9	3.4
Eu	2.1	1.5	1.9	1.45	1
Gd	8	5.5	5.8	4	2.7
Tb	1	1	1.02	0.7	0.52
Tm	0.8	0.7	0.7	0.7	0.2
Yb	3.8	3.8	3.6	2.8	2.2
Lu	0.68	0.6	0.44	0.5	0.45
Sc	32	48	33	27	27
Fe	5.5	8	7.2	4.2	3.5
Co	68	48	39	44	43
Ba	100	68			
Rb	5	1.2		60	70
Th	4	4	1	0.9	0.5
Nb	61	2			
Ta	2.8	0.18	0.43	0.35	0.22
Cr	185	120	15	50	46
Hf	4.7	2.5	4.3	3.3	2.5
Cs	0.5		1.4	1.2	1.5
Sr	205	120			
Y	40	32			
Zr	250	92			
Zr/Nb	4.1	46			
(Nb/La)N	1.64	0.42			
(La/Ta)N	0.76	1.51	2.25	2.21	2.93
(La/Yb)N	5.85	0.75	2.81	1.01	3.06

OIB affinity and MORB-like greenstones. There are also several samples with transitional characteristics.

Discussion

Four periods of volcanism associated with Vendian-Early Phanerozoic evolution of the Paleo-Asian Ocean were studied here: (1) Vendian (Kurai zone); (2) Early Cambrian (Katun zone); (3) Late Cambrian-Early Ordovician (Zasurin Formation) and (4) Late Devonian-Early Carboniferous (Chara belt). The entities of the study were possibly hot spot or plume-induced oceanic basalts incorporated in four Caledonian accretion-collision zones.

The Gorny Altai, North-West Altai and East Kazakhstan accretion-collision zones comprise rock units which formed over the oceanic crust of the Paleo-Asian Ocean. They were incorporated into accretionary wedges during its subduction under the Siberian continent and subsequent collision of the Altai-Mongolian terrane and Kazakhstan continent with the Siberian continent. The accretionary wedges are characterized by a sheeted structure, and consist of ophiolites from the basement of an island-arc and the rocks of a deformed oceanic crust (the Paleo-Asian oceanic plate).

Mid-oceanic ridges, oceanic plateaux and islands transported into the subduction zone (forming part of the subduction assemblage) were subsequently incorporated into the accretionary wedge complex. The collision and subduction of oceanic islands promoted reverse currents within the overriding accretionary wedge, resulting in exhumation of high-pressure rocks such as blueschists and eclogites. The fragments of paleoseamounts in the accretionary wedge are as a rule hosted by olistostromes together with island arc units (Dobretsov et al., 2003).

The Early Cambrian collision of Gondwana-derived terranes with the Siberian continent induced Early Caledonian accretion-collisional processes, exemplified by the Kurai and Katun zones in Gorny Altai. Fragments of a Vendian island arc, a Vendian-Early Cambrian accretionary wedge, and a Cambrian fore-arc basin have been preserved in this territory.

In the Late Cambrian-Early Ordovician, the Siberian continent and Gondwana-derived terranes collided, and induced subduction of the oceanic crust at the eastern side of the mid-oceanic ridge in the Paleo-Asian Ocean, and related formation of shear zones with a sheeted structure composed of oceanic sediments and basalts.

The Late Devonian-Early Carboniferous collision of the Siberian and Kazakhstan continents closed the easternmost branch of the Paleo-Asian Ocean and induced strike-slip faulting, collisional deformation and rotation of terranes. The Chara belt, which is composed of accretionary terranes, represents a strike-slip zone formed between the Kazakhstan and Siberian continents in the Late Paleozoic (Buslov et al., 2003).

Geochemical studies of four suites of basaltic rocks possessing OIB, OPB and MORB geochemical characteristics show that basalts derived from both enriched and depleted mantle sources and later incorporated in accretionary terranes may illustrate the history of hot-spot volcanism and its relation to the evolution of the Paleo-Asian Ocean. Most of the samples studied are tholeiitic and/or subalkaline basalts and alkaline basalts.

The Kurai accretionary wedge contains three kinds of basaltic rocks: OIB-type, N-MORB-type and T-MORB or OPB (Fig. 9A). Differences in trace element contents between those three types of rocks cannot be explained by fractional crystallization because the highest-TiO_2 rock has an intermediate MgO content (sample 154, Table 1). Therefore, we suggest that some of the Kurai basalts are of OIB origin, which is well correlated with their field occurrence and petrography. On the other hand, the Kurai basalts exhibit chondrite-normalized REE patterns with LREE-depletions similar to those of MORB. These patterns are inconsistent with formation in an oceanic island setting, as suggested by their structural occurrence and petrography.

The complex features of the Kurai basaltic rocks are

most similar to OPB. Typical oceanic plateaux are frequently accompanied by limestone (e.g., Saunders et al., 1996). Oceanic plateaux are composed of aphyric or porphyritic basalts with N-MORB to E-MORB petrochemical affinities. Most of the basalts examined are porphyritic, which can be explained by delayed eruption from depth, i.e. with stagnation in a shallow-level magma chamber (Nagahashi and Miyashita, 2002).

Returning to the four basalt suites, we can see that two types of REE patterns occur (Fig. 9): LREE-enriched and MORB- or OPB-like flat patterns. REE contents can be influenced by the degree of differentiation, the degree of partial melting and the source concentrations in the mantle reservoir. Light-REE abundances vary and are considerably enriched (La_N (ppm) 25–65 for Kurai, 35-55 for Katun, 100–160 for Zasurin, and 35–105 for Chara OIB samples) relative to chondrite, whereas heavy-REE abundances have much smaller ranges, from 6 to 13 times that of chondrite for Kurai and Katun, and 10 to 20 times for the Zasurin and Chara samples (Fig. 9). Moreover, there is a systematic correlation of increasing La/Yb ratio with increasing SiO_2 content (Tables 1, 2, 4, and 6).

Chondrite-normalized trace-element abundances identify three groups of greenstones: MORB-like, OIB and transitional between OIB and MORB (Fig. 11). Those with OIB affinities are qualitatively similar to those in other suites of alkaline and tholeiitic oceanic island basalts (Clague and Frey, 1982; Garcia et al., 1986; Frolova and Burikova, 1997; Ueda et al., 2000; Li et al., 2002). In multi-element diagrams, the Kurai samples display Sr enrichment relative to K that can be explained by low-grade alteration in sea-water following eruption in sea-floor environments (Figs. 10, 11). The Zasurin and Chara samples show negative Sr anomalies, possibly due to the fractionation of plagioclase. Most samples, except for several from the Katun wedge, display moderate to strong Nb-Ta depletion and clear enrichment in LILE (Fig. 10). The Nb-Ta depletions suggest fractionation of ilmenite and magnetite and their separation in the base of the crust. On the other hand, Nb and Ta depletions could also be source-related, i.e. the source could have experienced a previous melting episode. For all groups of basalts, transitions between basalt end members occur: from N-MORB, through E-MORB and T-MORB/OPB to OIB (Fig. 10). While regarding the petrology of the metabasalts based on their geochemical features, we must take into account the depth of the formation of basaltic melts. Most OIB-close melts are formed at a depth greater than 80 km.

There are two main models of oceanic basaltic volcanism sampling the Earth's mantle (Hofmann, 1997): one-reservoir and two-reservoir. The first is based on the idea of a chemically layered mantle, with an upper depleted and a lower undepleted (also called primitive) layer. The second is based on "whole-mantle convection" assuming that subducted lithosphere regularly or occasionally penetrates the 660 km boundary, and all plumes originate from the core-mantle boundary. This may happen when laterally migrating mid-oceanic ridges, which normally "sample" the uppermost mantle (i.e., the asthenosphere), occasionally intersect a plume, rising from the deeper mantle. In that case we may observe gradual transitions between OIB-like and MORB-like varieties. The trace element composition of melts also depends on the degree of melting.

In our case, the oceanic metabasalts from four areas of the Altai-Sayan display many common geochemical features. On one hand, the basalts under consideration could have been melted at different degrees of partial melting and at different depths. On the other hand, they could originated from one mantle source, but then been differently influenced and/or contaminated by the upper mantle matter; for example, a weakly depleted oceanic mantle could interact with upwelling plume melts. Rather high LILE and moderate Nb depletion may also suggest interaction between a mantle plume and a spinel-facies mantle source.

Conclusions

The Gorny Altai, North-West Altai and East Kazakhstan examples demonstrate that fragments of oceanic crust comprise not only ophiolitic rock units, but also paleo-oceanic island units, and are important features in the structure of foldbelts.

Our presented combined study of the fragments of oceanic crust involved in accretionary terranes lead us to conclude that hot-spot volcanism was active in the early stages of the Paleo-Asian oceanic evolution, in a period from the Vendian to the Early Carboniferous. Fragments of weakly to strongly differentiated varieties of oceanic and island-arc basalts preserved in accretion-collision zones provide information about chemical composition and petrology of volcanic rocks composing the greatest volume of the oceanic crust.

The geochemical data indicate that the Altai and East Kazakhstan metabasalts could have been formed at mid-oceanic ridges, oceanic islands or oceanic plateaux of the Paleo-Asian Ocean in Vendian to Early Carboniferous times.

The combined interpretation of structural, lithological, geochemical and biostratigraphic data shows that the Vendian-Cambrian oceanic lithosphere of the Paleo-Asian Ocean was structurally and compositionally similar to the present Pacific. Further detailed geochemical investigation would allow more complete reconstruction of the ancient oceans and a better understanding of the petrologic processes which resulted in formation of the paleo-oceanic crust.

Acknowledgments

We thank Prof. N.L. Dobretsov, Drs. N. V. Sennikov, O.T. Obut, N.N. Semakov and O.M. Turkina, all from UIGGM SB RAS, Prof. Y. Fujiwara, S. Okada, S. Maruyama and Dr. T. Ota for fruitful discussions and joint field missions, and Dr. V.A. Bobrov for REE and trace element determinations.

The research was sponsored in parts by funds from RFBR Grants No. 02-05-64627 and 03-05-64668. Prof. Shigenori Maruyama supported part of the field expenses. Dr. Andrei Izokh of the Institute of Geology, SBRAS, is thanked for constructive discussion of an early version of the manuscript. Constructive reviews by John Gamble and Hayato Ueda greatly improved this manuscript.

References

Ben-Avrahem, Z., Nur, A., Jones, D. and Cox, A. (1981) Continental accretion: from oceanic plateau to allochthonous terranes. Science, v. 213, pp. 47-54.

Berzin, N.A. and Dobretsov, N.L. (1994) Geodynamic evolution of Southern Siberia in Late Precambrian – Early Paleozoic time, In: Coleman, R.G. (Ed.), Reconstruction of the Paleo-Asian ocean. Utrecht, The Netherlands, pp. 53-70.

Buslov, M. M. and Watanabe, T. (1996) Intrasubduction collision and its role in the evolution of an accretionary wedge: the Kurai zone of Gorny Altai, Central Asia. Russian Geol. Geophys., v. 36, pp. 83-94.

Buslov, M.M., Saphonova, I.Yu. and Bobrov, V.A. (1998) New geochemical data on boninites from Kurai ophiolites, Gorny Altai. Dokl. RAN, v. 361, pp. 244-247.

Buslov, M.M., Saphonova, I.Yu and Bobrov, V.A. (1999) An exotic terrane of the Late Cambrian-Early Ordovician oceanic crust in the northwestern Gorny Altai (Zasurin Formation): structural position and geochemistry. Dokl. RAN, v. 368, pp. 650-654.

Buslov, M.M., Berzin, N.A., Dobretsov, N.L. and Simonov, V.A. (1993) Geology and tectonics of Gorny Altai. Novosibirsk, UIGGM Publ., Novosibirsk, 122p.

Buslov, M.M., Fujiwara, Y., Saphonova, I.Yu, Okada, Sh. and Semakov, N.N. (2000) The junction zone of the Gorny Altai and Rudny Altai terranes: structure and evolution. Russian Geol. Geophys., v. 41, pp. 377-390.

Buslov M.M., Watanabe T., Saphonova I.Yu., Iwata K., Travin, A. and Akiyama M. (2002) A Vendian-Cambrian island arc system of the Siberian continent in Gorny Altai (Russia, Central Asia), Gondwana Res., v. 5, pp. 781-800.

Buslov, M.M, Watanabe, T., Smirnova, L.V., Fujiwara, Y., Iwata, K., De Grave, J., Semakov, N.N., Travin, A.V., Kirjanova, A.P. and Kokh D.A. (2003) Role of strike-slip faults in Late Paleozoic-Early Mesozoic tectonics and geodynamics of the Altai-Sayan and East Kazakhstan folded zones. Russian Geol. Geophys., v. 44, pp. 49-75.

Buslov, M.M., Saphonova, I.Yu., Watanabe, T., Obut, O.T., Fujiwara, Y., Iwata, K., Semakov, N. N., Sugai, Y., Smirnova, L.V., Kazansky, A.Yu. and Itaya, T. (2001) Evolution of the Paleo-Asian Ocean (Altai-Sayan Region, Central Asia) and collision of possible Gondwana-derived terranes with the southern marginal part of the Siberian continent. J. Geosci., v. 5, pp. 203-224.

Chekhovich, V.D. (1997) On the accretion of oceanic rises. Geotektonika, v. 4, pp. 69-79 (in Russian).

Clague, D.A. and Frey, F.A. (1982) Petrology and trace element geochemistry of the Honolulu volcanic, Oahu; implication for the oceanic mantle below Hawaii. J. Petrol., v. 23, pp. 447-504.

Coleman, R.G. (1977) Ophiolites. Springer-Verlag, Berlin.

Dobretsov, N.L. and Zonenshain, L.P. (Eds.), (1985) Riphean-Paleozoic ophiolites of North Eurasia. Nauka, Novosibirsk (in Russian).

Dobretsov, N.L., Berzin, N.A. and Buslov, M.M. (1995) Opening and tectonic evolution of the Paleo-Asian Ocean. Int. Geol. Rev., v. 35, pp. 335-360.

Dobretsov, N.L., Buslov, M.M. and Uchio,Yu. (2003) Fragments of oceanic islands in accretion-collision areas of Gorny Altai and Salair, southern Siberia, Russia: early stages of continental crust growth of the Siberian continent in Vendian-Early Cambrian time. J. Asian Earth Sci. (accepted for publication).

Feigenson, M.D., Patino, L.C. and Carr, M.J. (1996) Constraints on partial melting imposed by rare earth element variations in Mauna Kea basalts. J. Geophys. Res., v. 101, pp. 11815-11829.

Floyd, P.A. (1989) Geochemical features of interaplate oceanic plateau basalts. In: Saunders, A.D. and Norry, M.J. (Eds.), Magmatism in the ocean basins. Geol. Soc. London Spec. Pub., v. 42, pp. 215-230.

Frolova, T.I. and Burikova, I.A. (1997) Magmatic formations in modern geotectonic environments. Moscow Univ. Press, 319p.

Garcia, M.O., Frey, F.A. and Grooms, D.G. (1986) Petrology of volcanic rocks from Kaula Island, Hawaii: implications for the origin of Hawaiian protoliths. Contrib. Mineral. Petrol., v. 94, pp. 461-471.

Gibsher, A.S., Esin, S.V., Izokh, A.E., Kireev, A.D. and Petrova, T.V. (1996) Cambrian diopside-bearing basalts from the Cheposh zone in Gorny Altai. Russian Geol. Geophys., v. 38, pp. 1760-1773.

Gusev, N.I. (1991) Reconstruction of geodynamic regimes for Precambrian and Cambrian volcanism in southeastern Gorny Altai. In: Kuznetsov, P.P. et al. (Eds.), Paleogeodynamics and formation of mineral-rich zones in South Siberia, pp. 32-54 (in Russian).

Hofmann, A.W. (1997) Mantle geochemistry: the message from oceanic volcanism. Nature, v. 385, pp. 219-229.

Hofmann, A.W. and Jochum, K.P. (1996) Source characteristics derived from very incompatible trace elements in Mauna Loa and Mauna Kea basalts, Hawaii Scientific Drilling Project. J. Geophys. Res., v. 101, pp. 11831-11839.

Humphris, S.E. and Thompson, G. (1978) Hydrothermal alteration of oceanic basalts by seawater. Geochim. Cosmochim. Acta, v. 42, pp. 107-125.

Iwata, K., Obut, O.T. and Buslov, M.M. (1997a) Devonian and Lower Carboniferous radiolaria from the Chara ophiolite belt, East Kazakhstan. News of Osaka Micropaleontologist, v. 10, pp. 27-32.

Iwata, K., Watanabe, T., Akiyama, M., Dobretsov, N.L. and Belyaev, S.Yu. (1994) Paleozoic microfossils from the Chara Belt (Eastern Kazakhstan). Russian Geol. Geophys., v. 35, pp. 125-130.

Iwata, K., Sennikov, N.V., Buslov, M.M., Obut, O.T., Shokalsky, S.P., Kuznetsov, S.A. and Ermikov, V.D. (1997b), Upper Cambrian-Early Ordovician age of the Zasur'ia basalt-chert-terrigenous formation (northwestern Gorny Altai). Russian Geol. Geophys., v. 38, pp. 1427- 1444.

Kay, R., Hubbard, N.J. and Gast, P.W. (1970) Chemical characteristics and origin of oceanic ridge volcanic rocks. J. Geophys. Res., v. 75, pp. 1585.

Li, X., Li, Zh.-X., Zhou, H., Liu, Y. and Kinny, P.D. (2002) U-Pb zircon geochronology, geochemistry and Nd isotopic study of Neoproterozoic bimodal volcanic rocks in the Kandigan Rift of South China: implications for the initial rifting of Rodinia. Precambrian Res., v. 113, pp. 135-154.

McDonough, W.F. and Sun, S. (1995) The composition of the Earth. Chem. Geol., v. 120, pp. 223-253.

Meschede, M. (1986) A method of discriminating between different types of Mid-Oceanic Ridge Basalts and continental tholeiites with the Nb-Zr-Y diagram. Chem. Geol., v. 56, pp. 207-218.

Mullen, E.D. (1983) $MnO/TiO_2/P_2O_5$: a minor element discriminant for basaltic rocks of oceanic environments and its implications for petrogenesis. Earth Planet. Sci. Lett., v. 62, pp. 53-62.

Miyashiro, A. (1973) The Troodos ophiolitic complex was probably formed in an island arc. Earth Planet. Sci. Lett., v. 19, pp. 218-224.

Nagahashi, T. and Miyashita, S. (2002) Petrology of the greenstones of the Lower Sorachi Group in the Sorachi-Yezo Belt, central Hokkaido, Japan, with special reference to discrimination between oceanic plateau basalts and mid-oceanic ridge basalts. The Island Arc, v. 11, pp. 122-141.

Pearce, J.A. (1982) Trace element characteristics of lavas from destructive plate boundaries. In: Thorpe, R.S. (Ed.), Andesites. John Wiley & Sons, Chichester, pp. 525-548.

Repina, L.N. and Romanenko, E.V. (1964) Trilobites and Lower Cambrian stratigraphy of Altai-Sayan folded area. Nauka, Moscow (in Russian), p. 74.

Rhodes, J.M. (1973) Major and trace element chemistry of basalts from Leg 9 of the Deep Sea Drilling Project. EOS, v. 54, pp. 1014-1015.

Rollinson, H.R. (1993) Using geochemical data: evaluation, presentation, interpretation. Longman Group UK Ltd., 352p.

Saunders, A.D. (1986) Geochemistry of basalts from the Nauru basin, Deep Sea Drilling Project Legs 61 and 89: Implications for the origin of oceanic flood basalts. In: Moberly, R., Schlanger, S.O. et al. (Eds.), Initial reports of the deep sea drilling project, U.S. govt. Printing Office, Washington DC, v. 89, pp. 499-517

Sennikov, N.V., Iwata, K., Ermikov, V.D., Obut, O.T. and Khlebnikova, T.V. (2003) Oceanic sedimentation settings and fauna associations in the Paleozoic on the southern framing of the West Siberian Plate. Russian Geol. Geophys., v. 44, pp. 156-171.

Simonov, V.A., Dobretsov, N.L. and Buslov, M.M. (1994) Boninite series in structures of the Paleo-Asian Ocean. Russian Geo. and Geophys., v. 35, pp. 182-199.

Sun, S. and McDonough, W.F. (1989) Chemical and isotopic systematics of oceanic basalts: Implications for mantle composition and processes. In: Saunders, A.D. and Norry, M.J. (Eds.), Magmatism in the ocean basins. Geol. Soc. London. Spec. Publ., v. 42, pp. 313-345.

Tatsumi, Y., Shinjoe, H., Ishizuka, H., Sager, W.W. and Klaus, A. (1998) Geochemical evidence for a mid-Cretaceous superplume. Geology, v. 26, pp. 151-154.

Terleev, A.A. (1991) Stratigraphy of Vendian-Cambrian sediments of the Katun anticline (Gorny Altai). In: Khomentovskiy, V.V. (Ed.), Late Precambrian and Early Paleozoic of Siberia. UIGGM Publ., Novosibirsk, pp. 82-106 (in Russian).

Terleev, A.A., Luchinina, V.A., Sosnovskaya, O.V., Bagmed, G.N. and Kraevskii, B.G. (2002) Calcareous algae and the lowest Cambrian border in western Altai-Sayan. In: Letnikov, F.A. (Ed.), Geology, geochemistry and geophysics at the boundary between the XX and XXI centuries, IZK Publ., Irkutsk, pp. 131-133.

Uchio, Yu., Isozaki, Yu., Nohda, S., Kawahata, H., Ota T., Buslov, M.M. and Maruyama, Sh. (2001) The Vendian to Cambrian Paleo-environment in shallow mid-ocean: stratigraphy of Vendo-Cambrian seamount-top limestone in the Gorny Altai Mountains, Southern Russia. Gondwana Res., v. 4, pp. 47-48.

Ueda, H., Kawamura, M. and Niida, K. (2000) Accretion and tectonic erosion processes revealed by the mode of occurrence and geochemistry of greenstones in the Cretaceous accretionary complexes of the Idonappu zone, southern central Hokkaido, Japan. The Island Arc, v. 9, pp. 237-257.

Watanabe, T., Buslov, M.M. and Koitabashi, S. (1993) Comparison of arc-trench systems in the Early Paleozoic Gorny Altai and the Mesozoic-Cenozoic of Japan. In: Coleman, R.G. (Ed.), Reconstruction of the Paleo-Asian Ocean, VSP Intern. Sci. Publ., the Netherlands, pp. 160-177.

Wedepohl, L. (1981) Tholeiitic basalts from spreading ocean ridges: the growth of the oceanic crust. Naturwissenchaften, v. 68, pp. 26-52.

Wilson, M. (1989) Igneous petrogenesis. Chapman & Hall, London.

Winchester, J.A. and Floyd, P.A. (1977) Geochemical discrimination of different magma series and their differentiation products using immobile elements. Chem. Geol., v. 20, pp. 325-343.

Wood, D.A., Joron, J.L. and Treuil, M. (1979) A re-appraisal of the use of trace elements to classify and discriminate between magma series erupted in different tectonic settings. Earth Planet. Sci. Lett., v. 45, pp. 326-336.

Zonenshain, L.P., Kuzmin, M.I. and Natapov, L.M. (1990) Geology of the USSR: A plate tectonic synthesis. Geodynamic Monograph, Amer. Geophys. Union, Washington, 242p.